

Dynamic Quantile Function Models

Wilson Ye Chen¹, Gareth W. Peters², Richard H. Gerlach³, and Scott A. Sisson⁴

¹University of Technology Sydney

¹Australian Research Council Centre of Excellence for Mathematical and Statistical Frontiers

²Department of Statistical Science, University College London

³Discipline of Business Analytics, University of Sydney

⁴School of Mathematics and Statistics, University of New South Wales

July 9, 2017

Abstract

We offer a novel way of thinking about the modelling of the time-varying distributions of financial asset returns. Borrowing ideas from symbolic data analysis, we consider data representations beyond scalars and vectors. Specifically, we consider a quantile function as an observation, and develop a new class of dynamic models for quantile-function-valued (QF-valued) time series. In order to make statistical inferences and account for parameter uncertainty, we propose a method whereby a likelihood function can be constructed for QF-valued data, and develop an adaptive MCMC sampling algorithm for simulating from the posterior distribution. Compared to modelling realised measures, modelling the entire quantile functions of intra-daily returns allows one to gain more insight into the dynamic structure of price movements. Via simulations, we show that the proposed MCMC algorithm is effective in recovering the posterior distribution, and that the posterior means are reasonable point estimates of the model parameters. For empirical studies, the new model is applied to analysing one-minute returns of major international stock indices. Through quantile scaling, we further demonstrate the usefulness of our method by forecasting one-step-ahead the Value-at-Risk of daily returns.

Keywords: symbolic data, time series, MCMC, quantile function, g-and-h, Value-at-Risk

1 Introduction

Modelling the time-varying distribution of financial returns has been an interest to many authors in the past three decades, beginning with Engle (1982). The increasing availability of high-frequency data has presented new challenges, namely, effectively making use of the information contained in the intra-daily observations at a reasonable computational cost. One approach is to work with a daily aggregate such as realised variance or realised range (Andersen et al., 2003; Martens and van Dijk, 2007; Gerlach and Chen, 2014). These realised measures are single numerically valued summaries of intra-daily data. Another approach is to consider data representations beyond scalars and vectors. For example, Arroyo et al. (2011), González-Rivera and Arroyo (2012), and González-Rivera and Lin (2013) have considered smoothing methods and autoregressive models for interval-valued

and histogram-valued time series. Interval-valued and histogram-valued data can be considered symbolic data. As symbolic data analysis (SDA) is concerned with the modelling of data summaries, it is naturally suited for dealing with massive datasets.

We consider a quantile function as an observation, and develop a class of dynamic models for quantile-function-valued time series. There are several motivations for making quantile function the symbolic representation: the distribution of a random variable is characterised by its quantile function; direct modelling of quantile functions can be more convenient in applications where the quantity of interest is a quantile; a number of very flexible distributions, such as the generalised λ distribution and the g-and-h distribution, are defined only through their quantile functions. As an illustration, we choose the quantile function of the g-and-h distribution. The g-and-h distribution is able to approximate a broad spectrum of distributions with different values of kurtosis and skewness, however it is somewhat less explored in the literature, perhaps due to the fact that it does not have a closed form density function. We show that the g-and-h quantile function can be effectively fitted via the method of L-moments. Defining likelihood functions for quantile-function-valued data is a non-trivial task. Le-Rademacher and Billard (2011) have proposed a general method for finding a likelihood function for symbolic data, by mapping a symbolic observation into \mathbb{R}^p . Using their framework, the likelihood functions for the proposed generalised autoregressive quantile function models are defined, which allow for the subsequent Bayesian estimation. In the empirical study, we model the time series of quantile functions of high-frequency financial returns, and demonstrate the usefulness of our method by forecasting one-step-ahead the extreme quantiles of intra-daily returns. Furthermore, through a simple empirical scaling rule, we are able to forecast one-step-ahead the value-at-risk of daily returns.

2 Dynamic quantile function models

2.1 Preliminaries

We consider a *quantile function* as an observation. Let (Ω, \mathcal{A}, P) be a probability space, where Ω is the reference space with $\omega \in \Omega$ being an element, \mathcal{A} is a σ -algebra of subsets of Ω , and P is a probability measure over \mathcal{A} . Let X be a real-valued function of two variables, $u \in [0, 1]$ and $\omega \in \Omega$. If u is fixed, $X(u, \cdot)$ is a (real-valued) random variable defined on (Ω, \mathcal{A}, P) . If ω is fixed, $X(\cdot, \omega)$ is a real-valued function on $[0, 1]$ belonging to some function space \mathbb{S} . If \mathbb{S} is restricted to be a subset of all quantile functions, i.e.,

$$\mathbb{S} \subseteq \{(Q: [0, 1] \rightarrow \mathbb{R}): Q(a) < Q(b), \forall a < b\}, \quad (1)$$

and ω is allowed to vary, then X is called a *quantile-function-valued (QF-valued) random variable*. A *QF-valued discrete-time stochastic process* is a set of QF-valued random variables index by integers. We use the notation $\{X_t\}$ to refer to such process. I.e., $\{X_t\}$ is the abbreviated notation for $\{X_t: t \in \mathbb{Z}\}$.

We can view a dynamic model for *QF-valued time series* in general as

$$\tilde{X}_t = \rho(\{X_s: s \leq t-1\}), \quad \tilde{X}_t \in \mathbb{S}, \quad (2)$$

where \tilde{X}_t is an one-step-ahead forecast generated by a function ρ of the set of all QF-valued observations up to $t-1$. Given a sample of QF-valued realisations $\{X_1, \dots, X_T\}$, a forecasting tool can be found by first defining some distance measure between two quantile functions $d: \mathbb{S} \times \mathbb{S} \rightarrow \mathbb{R}$, then minimising the sum of one-step-ahead forecast errors $\sum_{t=1}^T d(\tilde{X}_t, X_t)$ with respect to ρ . If ρ is parameterised by a vector θ_ρ , then an estimate of ρ corresponds to a solution to an optimisation problem over the space of θ_ρ . A generative model can be constructed by defining a conditional distribution $F_{X,t}$ such that

$$X_t | \mathcal{G}_{t-1} \sim F_{X,t}, \quad (3)$$

where $\mathcal{G}_{t-1} = \sigma(\{X_s: s \leq t-1\})$ denotes the smallest σ -algebra containing the past observations of the process, and represents the available information at $t-1$. The filtration \mathcal{G}_{t-1} is referred to as the *natural filtration*. The forecast \tilde{X}_t can then be taken as a function of the predictive distribution $F_{X,t}$. Looking for a generative model is a more challenging task than building a forecasting tool, as the notion of a distribution function defined on a function space is in general not straightforward. A detailed explanation can be found in Delaigle and Hall (2010) and Cuevas (2014).

The idea adopted in this paper is to develop a generative model for a quantile-function-valued time series indirectly, by first finding a suitable low-dimensional parameterisation for the observed quantile functions, and then specifying a generative model for the time series of mapped low-dimensional vectors. The strategy of indirectly modelling the symbolic observations through the modelling of their mapped vectors is proposed by Le-Rademacher and Billard (2011), where the authors applied it to interval-valued and histogram-valued data.

Suppose that we define a parameterisation of X_t that maps a symbolic observation to a p -dimensional vector,

$$\mathcal{M}: \mathbb{S} \rightarrow \mathbb{R}^p, \quad (4)$$

so that we are able to obtain a vector

$$\xi_t = \mathcal{M}(X_t), \quad (5)$$

and define a conditional distribution F_t on \mathbb{R}^p such that

$$\xi_t | \mathcal{F}_{t-1} \sim F_t, \quad (6)$$

where $\mathcal{F}_{t-1} = \sigma(\{\xi_s: s \leq t-1\})$. If the mapping \mathcal{M} is one-to-one, the distribution F_t corresponds to a generative model for X_t , namely, the push-forward of F_t under \mathcal{M}^{-1} . We can also define the one-step-ahead forecast to be the quantile function whose mapped

vector is the conditional expectation of ξ_t ,

$$\tilde{X}_t = \mathcal{M}^{-1}(\mathbb{E}[\xi_t | \mathcal{F}_{t-1}]). \quad (7)$$

The *modelling task* is then to define the collection $\{\mathbb{S}, \mathcal{M}, F_t\}$. Notice that the mapping \mathcal{M} is non-unique and the properties of the model greatly depends on its choice. In the subsequent sections, we will introduce one particular choice of \mathcal{M} based on the g-and-h family of distributions.

2.2 The g-and-h family of distributions

We adopt a parametric approach and assume that X_t has the functional form of the quantile function of a g-and-h distribution, that is, we define the symbol set as $\mathbb{S} = \{\text{g-and-h quantile functions}\}$. The g-and-h family of distributions was first introduced by Tukey (1977) and further developed by Martinez and Iglewicz (1984) and Hoaglin (1985). It is generated by a transformation of a standard normal random variable which allows for asymmetry and heavy tails. Specifically, let z be a standard normal random variable, and let $a \in \mathbb{R}$, $b \in (0, \infty)$, $g \in \mathbb{R}$, and $h \in [0, \infty)$ be constants. The random variable y is said to follow a g-and-h distribution if it is given by the transformation,

$$y = a + bG(z)H(z)z, \quad (8)$$

where

$$G(z) = \frac{\exp(gz) - 1}{gz} \quad (9)$$

and

$$H(z) = \exp\left(\frac{hz^2}{2}\right). \quad (10)$$

Note that the same transformation can be applied to any “base” random variable. It can be seen from (8) that a and b account for location and scale, respectively. It can be checked from (9) that the reshaping function G is bounded from below by zero, that it is either monotonically increasing or monotonically decreasing for g being, respectively, positive or negative, and that by rewriting it as its series expansion,

$$G(z) = 1 + \frac{gz}{2!} + \frac{(gz)^2}{3!} + \frac{(gz)^3}{4!} + \dots, \quad (11)$$

G is equal to one at zero for all g . Thus G generates asymmetry by scaling z differently for different side of zero via the parameter g . Furthermore, as $G(z; g) = G(-z; -g)$, the sign of g affects only the direction of skewness. For $g = 0$, by equation (11), the constant function $G(z) = 1$ is obtained, and thus the symmetry remains unmodified. For $h > 0$, H is a strictly convex even function with $H(0) = 1$, and thus it generates heavy tails by scaling upward the tails of z while preserving the symmetry. When $h = 0$, the transformation given by (8) generates the subfamily of g-distributions, which coincides with the family of shifted log-normal distributions for $g > 0$. When $g = 0$, the transformation generates the subfamily of h-distributions, which is symmetric and has heavier tails than normal

distributions.

2.3 The gh-DQF model

As the transformation given by (8) is monotonically increasing as long as $h > 0$, the quantile function of the g-and-h distributions is explicitly available. As discussed in Section 2.2, we assume that X_t is the quantile function of a g-and-h distribution,

$$X_t(u) = \begin{cases} a_t + b_t \frac{\exp(g_t Z(u)) - 1}{g_t} \exp\left(\frac{h_t Z(u)^2}{2}\right) & \text{if } g_t \neq 0, \\ a_t + b_t Z(u) \exp\left(\frac{h_t Z(u)^2}{2}\right) & \text{if } g_t = 0, \end{cases} \quad (12)$$

where Z is the quantile function of the standard normal distribution, $a_t \in \mathbb{R}$, $b_t \in (0, \infty)$, $g_t \in \mathbb{R}$, and $h_t \in [0, \infty)$ are parameters responsible for location, scale, asymmetry, and heavy-tailedness, respectively. We then choose the parameterisation \mathcal{M} to be

$$\boldsymbol{\xi}_t = (\xi_{1,t}, \xi_{2,t}, \xi_{3,t}, \xi_{4,t}) = (a_t, b_t^*, g_t, h_t), \quad (13)$$

where $b_t^* = \log(b_t)$. As b_t is a positive scale parameter, its natural logarithm is used for subsequent modelling convenience.

2.4 Estimating the g-and-h parameters

Up until this point, we have been treating $\{X_1, \dots, X_T\}$ as data that are directly observable. However, infinite dimensional quantile functions can never be observed in reality; only the realised order statistics are observed. QF-valued observations must therefore be constructed using scalar-valued observations. Let $\{\mathbf{y}_1, \dots, \mathbf{y}_T\}$ denote a sequence of vectors, where, for each $t \in \{1, \dots, T\}$, the vector $\mathbf{y}_t \in \mathbb{R}^{n_t}$ denotes a sample of n_t scalar-valued observations. One way of constructing the sequence $\{\mathbf{y}_t\}$ is by partitioning a long time series $\{y_1, \dots, y_{N_T}\}$ into T consecutive pieces, where $N_t = \sum_{i=1}^t n_i$, so that $\mathbf{y}_t = (y_{N_{t-1}+1}, \dots, y_{N_t})$ contains the n_t observations belong to the t th piece, as illustrated in Figure 1.

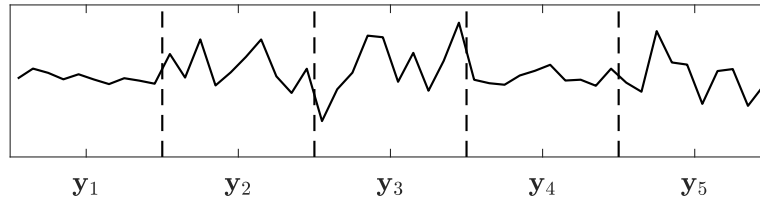


Figure 1: Illustration of constructing a sequence of vectors $\{\mathbf{y}_t\}$ by cutting a long time series into pieces.

Let $S : \mathbb{R}^n \rightarrow \mathbb{S}$, for $n \in \mathbb{N}$, denote a symbol constructor. The sequence $\{X_1, \dots, X_T\}$ is obtained via

$$X_t = S(\mathbf{y}_t), \quad (14)$$

for each $t \in \{1, \dots, T\}$. In the case where \mathbb{S} is the set of g-and-h quantile functions, the symbol constructor S corresponds to an estimator for the parameters of the g-and-h quantile function. Several studies in the statistics literature have been performed on the estimation of parametric quantile functions, such as those based on numerical likelihood (Rayner and MacGillivray, 2002; Hossain and Hossain, 2009), matching quantiles (Xu et al., 2014), matching moments (Headrick et al., 2008), and Bayesian methods (Haynes and Mengersen, 2005; Peters and Sisson, 2006; Allingham et al., 2009). We employ a method developed by Peters et al. (2016) based on L-moments which shows favorable statistical properties while being computationally simple compared to previously proposed methods. It is shown via simulations that the parameter estimates from the L-moment method have the smallest mean-squared-error compared to those from methods based on numerical likelihood, conventional moments, and quantiles. For the rest of section, we briefly summarise the L-moment method. Since we are concerned with the estimation of a single quantile function for a given time-period, to simplify notation, the subscript t is dropped for the rest of the section whenever clarity is not lost.

L-moments are defined by Hosking (1990) to be certain linear combinations of expectations of order statistics. Specifically, let $y_{(1)} \leq y_{(2)} \leq \dots \leq y_{(n)}$ denote a sample of ordered observations. For $k \in \{1, 2, \dots\}$, the k -th L-moment is defined as

$$l_k = \frac{1}{k} \sum_{i=0}^{k-1} (-1)^i \binom{k-1}{i} \mathbb{E}[y_{(k-i)}]. \quad (15)$$

The connection between L-moments and a quantile function becomes apparent when L-moments are expressed as projections of a quantile function onto a sequence of orthogonal polynomials that forms a basis of L^2 ;

$$l_k = \int_0^1 X(u) L_{k-1}(u) du, \quad (16)$$

where L_k is the k -th shifted Legendre polynomial in the sequence. Compared to classical moments, L-moments are able to characterise a wider range of distributions as all L-moments of a distribution exist if and only if the mean exists. Furthermore, a distribution with finite mean is uniquely characterised by its sequence L-moments. Using the representation of (16), the first four L-moments are given by

$$\begin{aligned} l_1 &= \int_0^1 X(u) du, \\ l_2 &= \int_0^1 X(u)(2u-1) du, \\ l_3 &= \int_0^1 X(u)(6u^2-6u+1) du, \\ l_4 &= \int_0^1 X(u)(20u^3-30u^2+12u-1) du. \end{aligned} \quad (17)$$

The location and scale invariant L-moment ratios, τ_3 and τ_4 , analogous to the classical skewness and kurtosis, respectively termed L-skewness and L-kurtosis in Hosking (1990),

are defined as

$$\begin{aligned}\tau_3 &= l_3/l_2, \\ \tau_4 &= l_4/l_2.\end{aligned}\tag{18}$$

Unlike the classical skewness and kurtosis, L-skewness and L-kurtosis are bounded, with $\tau_3 \in (-1, 1)$ and $\tau_4 \in [\frac{1}{4}(5\tau_3^2 - 1), 1)$. The boundedness of L-moment ratios makes them easy to interpret.

The sample L-moments, also known as L-statistics, are unbiased estimates of L-moments based on the order statistics of an observed sample. In particular, the first four sample L-moments are given by

$$\begin{aligned}\hat{l}_1 &= \hat{M}_0, \\ \hat{l}_2 &= 2\hat{M}_1 - \hat{M}_0, \\ \hat{l}_3 &= 6\hat{M}_2 - 6\hat{M}_1 + \hat{M}_0, \\ \hat{l}_4 &= 20\hat{M}_3 - 30\hat{M}_2 + 12\hat{M}_1 - \hat{M}_0,\end{aligned}\tag{19}$$

where \hat{M}_k is the k -th sample probability weighted moment (Greenwood et al., 1979), given by

$$\hat{M}_k = \begin{cases} \frac{1}{n} \sum_{i=1}^n y_{(i)} & \text{if } k = 0 \\ \frac{1}{n} \sum_{i=1}^n \frac{(i-1)(i-2)\dots(i-k)}{(n-1)(n-2)\dots(n-k)} y_{(i)} & \text{if } k > 0. \end{cases}\tag{20}$$

The estimates of g and h are simultaneously found by iteratively minimising the objective

$$(\tau_3 - \hat{\tau}_3)^2 + (\tau_4 - \hat{\tau}_4)^2,\tag{21}$$

subject to $0 \leq h < 1$, where $\hat{\tau}_3 = \hat{l}_3/\hat{l}_2$ is the sample L-skewness and $\hat{\tau}_4 = \hat{l}_4/\hat{l}_2$ is the sample L-kurtosis. The integrals in (17) are available in closed-form for the g-and-h quantile function (Peters et al., 2016), or they can be obtained numerically using one-dimensional adaptive quadrature. Given the estimates of g and h , the estimates of b and a are given by

$$\begin{aligned}b &= \hat{l}_2/l_2, \\ a &= \hat{l}_1 - bl_1.\end{aligned}\tag{22}$$

2.5 Modelling the conditional joint distribution of $\boldsymbol{\xi}_t$

We assume a flexible model in which the conditional joint distribution of $\boldsymbol{\xi}_t$ is defined by a copula and univariate conditional marginal distributions, denoted by

$$\boldsymbol{\xi}_t | \mathcal{F}_{t-1} \sim F_t = C(F_{1,t}, \dots, F_{4,t}),\tag{23}$$

where $C : [0, 1]^4 \rightarrow [0, 1]$ is the copula function that maps the conditional marginal distributions $\{F_{i,t}\}$ to the conditional joint distribution F_t . While it would be interesting to investigate the choice of C , for simplicity, we let C be the Student-t copula (Demarta and McNeil, 2005). Let $u_{i,t} = F_{i,t}(\xi_{i,t})$ and $\mathbf{u}_t = (u_{1,t}, \dots, u_{4,t})$. The conditional joint density

of ξ_t implied by the distribution function in (23) is

$$f_t(\xi_t) = c(\mathbf{u}_t) \prod_{i=1}^4 f_{i,t}(\xi_{i,t}), \quad (24)$$

where c is the Student-t copula density and $f_{i,t}(\xi_{i,t})$ is the conditional marginal density. The t copula density is given by

$$c(\mathbf{u}_t) = \frac{f_{\text{MSt}}(F_{\text{St}}^{-1}(u_{1,t}; \nu), \dots, F_{\text{St}}^{-1}(u_{4,t}; \nu); \mathbf{R}, \nu)}{\prod_{i=1}^4 f_{\text{St}}(F_{\text{St}}^{-1}(u_{i,t}; \nu); \nu)}, \quad (25)$$

where f_{MSt} is the multivariate t density parameterised a correlation matrix \mathbf{R} and degree-of-freedom ν , f_{St} is the univariate t density with ν degree-of-freedom, and F_{St}^{-1} is the univariate t distribution function with ν degree-of-freedom.

2.5.1 Conditional marginal distribution of a_t , b_t^* , and g_t

We model the conditional marginal distributions $F_{i,t}$ for $i \in \{1, 2, 3\}$, which correspond to the parameters a_t , b_t^* , and g_t , as follows.

$$\begin{aligned} \xi_{i,t} &= \mu_{i,t} + \epsilon_{i,t}, \\ \epsilon_{i,t} &= \sigma_{i,t} v_{i,t}, \\ v_{i,t} &\sim F_{\text{skt}}(\cdot; \eta_i, \lambda_i), \\ \mu_{i,t} &= \delta_i + \psi_i \xi_{i,t-1} + \phi_i \mu_{i,t-1}, \\ \sigma_{i,t}^2 &= \omega_i + \alpha_i \epsilon_{i,t-1}^2 + \beta_i \sigma_{i,t-1}^2. \end{aligned} \quad (26)$$

The innovation $v_{i,t}$ is generated from the skewed Student t distribution of Hansen (1994), denoted by $F_{\text{skt}}(\cdot; \eta_i, \lambda_i)$, where $\eta_i \in (2, \infty)$ is the degree-of-freedom parameter and $\lambda_i \in (-1, 1)$ the asymmetry parameter. The special cases $F_{\text{skt}}(\cdot; \eta_i, 0)$ and $F_{\text{skt}}(\cdot; \infty, 0)$ are the Student t and the standard normal distributions, respectively. Furthermore, the skewed t distribution is standardised so that $\mathbb{E}(v_{i,t}) = 0$ and $\text{Var}(v_{i,t}) = 1$. More properties of Hansen's skewed t distribution can be found in Jondeau and Rockinger (2003). The model in (26) implies that the mean and variance of the conditional marginal distribution $F_{i,t}$ are given by $\mathbb{E}(\xi_{i,t} | \mathcal{F}_{t-1}) = \mu_{i,t}$ and $\text{Var}(\xi_{i,t} | \mathcal{F}_{t-1}) = \sigma_{i,t}^2$, respectively. The dynamic properties of both $\{\mu_{i,t}\}$ and $\{\sigma_{i,t}^2\}$ are characterised by an extended form of exponential smoothing (Bosq, 2015). For the conditional variance to be positive, the conditions $\omega_i > 0$, $\alpha_i \geq 0$, and $\beta_i \geq 0$ are sufficient. Given that the positivity conditions are satisfied, the process $\xi_{i,t}$ is covariance stationary if $-1 < \psi_i + \phi_i < 1$ and $\alpha_i + \beta_i < 1$.

2.5.2 The family of Apatosaurus distributions

The tail shape parameter h_t must be non-negative for the transformation in (8) to be monotonically increasing in z_u and thus one-to-one. It can be challenging to model the conditional distribution of h_t or an obvious transformation of it, because h_t can become empirically very close to zero for many days. Furthermore h_t can also become very large

(close to 0.5) occasionally, for example, on days the so called “flash-crashes” occur. For the above reasons, we develop a novel family of distributions, termed the Apatosaurus family, for the modelling of h_t , which shows a good fit of the data empirically.

The Apatosaurus is a family of non-negative distributions constructed using a mixture of a truncated-skewed-t and an Exponential distribution. Depending on its parameters, the distribution can take on a variety of general shapes including having no mode, one mode, and one mode and one antimode. Notably, the Halphen distribution system (Perreault et al., 1999a,b) is able to take on a qualitatively similar set of shapes, however for our purpose of modelling h_t , the Apatosaurus distributions show a better fit to the data compared to the Halphen system.

Density We say that the random variable $h \sim F_{\text{Apat}}(h; \mu, \sigma, \eta, \lambda, \iota, w)$ if its density is given by

$$f_{\text{Apat}}(h; \mu, \sigma, \eta, \lambda, \iota, w) = w f_{\text{TrSkt}}(h; \mu, \sigma, \eta, \lambda) + (1 - w) f_{\text{Exp}}(h; \iota) \quad (27)$$

for $h \in [0, \infty)$, where f_{TrSkt} and f_{Exp} are the density functions of a truncated-skewed-t distribution and an Exponential distribution, and $w \in [0, 1]$ is the mixing weight.

The truncated-skewed-t distribution has the following density function.

$$f_{\text{TrSkt}}(h; \mu, \sigma, \eta, \lambda) = \frac{f_{\text{Skt}}(h; \mu, \sigma, \eta, \lambda)}{1 - F_{\text{Skt}}(0; \mu, \sigma, \eta, \lambda)}, \quad (28)$$

where f_{Skt} and F_{Skt} are the density and distribution functions of the skewed-t distribution of Hansen (1994), parameterised by its mode μ and scale σ in addition to the asymmetry and degree-of-freedom parameters, η and λ . The density function of skewed-t distribution f_{Skt} is given by

$$f_{\text{Skt}}(h; \mu, \sigma, \eta, \lambda) = \begin{cases} \frac{c}{\sigma} \left[1 + \frac{1}{\eta - 2} \left(\frac{h - \mu}{\sigma(1 - \lambda)} \right)^2 \right]^{-(\eta+1)/2} & \text{if } h < \mu, \\ \frac{c}{\sigma} \left[1 + \frac{1}{\eta - 2} \left(\frac{h - \mu}{\sigma(1 + \lambda)} \right)^2 \right]^{-(\eta+1)/2} & \text{if } h \geq \mu, \end{cases} \quad (29)$$

where $\sigma \in (0, \infty)$, $\eta \in (2, \infty)$, $\lambda \in (-1, 1)$, and

$$c = \frac{\Gamma\left(\frac{\eta+1}{2}\right)}{\sqrt{\pi(\eta-2)}\Gamma\left(\frac{\eta}{2}\right)}. \quad (30)$$

The distribution function F_{Skt} can be derived in a similar manner to Proposition 1 of Jondeau and Rockinger (2003), and is given by

$$F_{\text{Skt}}(h; \mu, \sigma, \eta, \lambda) = \begin{cases} (1 - \lambda) F_{t, \eta} \left(\frac{h - \mu}{\sigma(1 - \lambda)} \sqrt{\frac{\eta}{\eta - 2}} \right) & \text{if } h < \mu, \\ (1 + \lambda) F_{t, \eta} \left(\frac{h - \mu}{\sigma(1 + \lambda)} \sqrt{\frac{\eta}{\eta - 2}} \right) - \lambda & \text{if } h \geq \mu, \end{cases} \quad (31)$$

where $F_{t, \eta}$ is the distribution function of the t-distribution with η degrees-of-freedom.

The density function of the Exponential distribution in equation (27) is given by

$$f_{\text{Exp}}(h; \iota) = \frac{1}{\iota} \exp\left(-\frac{h}{\iota}\right), \quad (32)$$

where $\iota \in (0, \infty)$ is the mean parameter.

Mean The mean of the truncated-skewed-t distribution can be derived by noticing the following equivalence.

$$\begin{aligned} m_{\text{TrSkt}} &= \frac{1}{1 - F_{\text{Skt}}(0; \mu, \sigma, \eta, \lambda)} \int_0^\infty h f_{\text{Skt}}(h; \mu, \sigma, \eta, \lambda) dh \\ &= \frac{1}{1 - F_{\text{Skt}}(-\mu; 0, \sigma, \eta, \lambda)} \int_{-\mu}^\infty h f_{\text{Skt}}(h; 0, \sigma, \eta, \lambda) dh + \mu. \end{aligned} \quad (33)$$

The integral can then be written as

$$\int_{-\mu}^\infty h f_{\text{Skt}}(h; 0, \sigma, \eta, \lambda) dh = \int_{-\mu}^0 h f_{\text{Skt}}(h; 0, \sigma, \eta, \lambda) dh + \int_0^\infty h f_{\text{Skt}}(h; 0, \sigma, \eta, \lambda) dh. \quad (34)$$

Assuming that $\mu \in [0, \infty)$ and using the substitution

$$u(h) = 1 + \frac{1}{\eta - 2} \left(\frac{h}{\sigma(1 - \lambda)} \right)^2, \quad (35)$$

the first integral is given by

$$\begin{aligned} \int_{-\mu}^0 h f_{\text{Skt}}(h; 0, \sigma, \eta, \lambda) dh &= \frac{1}{2} c \sigma (1 - \lambda)^2 (\eta - 2) \int_{u(-\mu)}^1 u^{-(\eta+1)/2} du \\ &= -\frac{1}{2} c \sigma (1 - \lambda)^2 (\eta - 2) \int_1^{u(-\mu)} u^{-(\eta+1)/2} du \\ &= -c \sigma (1 - \lambda)^2 \left(\frac{\eta - 2}{\eta - 1} \right) \left[1 - u(-\mu)^{(1-\eta)/2} \right]. \end{aligned} \quad (36)$$

Using the substitution

$$u(h) = 1 + \frac{1}{\eta - 2} \left(\frac{h}{\sigma(1 + \lambda)} \right)^2, \quad (37)$$

the second integral in (34) is given by

$$\begin{aligned} \int_0^\infty h f_{\text{Skt}}(h; 0, \sigma, \eta, \lambda) dh &= \frac{1}{2} c \sigma (1 + \lambda)^2 (\eta - 2) \int_1^\infty u^{-(\eta+1)/2} du \\ &= c \sigma (1 + \lambda)^2 \left(\frac{\eta - 2}{\eta - 1} \right). \end{aligned} \quad (38)$$

Thus,

$$m_{\text{TrSkt}} = \frac{c \sigma \left(\frac{\eta-2}{\eta-1} \right) \{ (1 + \lambda)^2 - (1 - \lambda)^2 [1 - u(-\mu)^{(1-\eta)/2}] \}}{1 - F_{\text{Skt}}(-\mu; 0, \sigma, \eta, \lambda)} + \mu, \quad (39)$$

where

$$u(-\mu) = 1 + \frac{1}{\eta - 2} \left(\frac{-\mu}{\sigma(1 - \lambda)} \right)^2. \quad (40)$$

The mean for $\mu \in (-\infty, 0)$ can also be derived using the substitution given by (37), however it is natural for most applications to restrict the mode the the *pre-truncated* skewed-t distribution to be non-negative, i.e., $\mu \in [0, \infty)$.

The mean of the Exponential distribution is simply

$$m_{\text{Exp}} = \iota. \quad (41)$$

It follows from the density function in (27) that the mean of the Apatosaurus distribution is given by

$$m_{\text{Apat}} = wm_{\text{TrSkt}} + (1 - w)m_{\text{Exp}}. \quad (42)$$

Distribution function The distribution function of the Apatosaurus distribution is given by

$$F_{\text{Apat}}(h; \mu, \sigma, \eta, \lambda, \iota, w) = wF_{\text{TrSkt}}(h; \mu, \sigma, \eta, \lambda) + (1 - w)F_{\text{Exp}}(h; \iota), \quad (43)$$

where F_{TrSkt} and F_{Exp} are the distribution functions of a truncated-skewed-t distribution and an Exponential distribution. We can straightforwardly derive the distribution function of the truncated-skewed-t distribution as follows.

$$\begin{aligned} F_{\text{TrSkt}}(h; \mu, \sigma, \eta, \lambda) &= \int_0^h f_{\text{TrSkt}}(y; \mu, \sigma, \eta, \lambda) dy \\ &= \frac{\int_0^h f_{\text{Skt}}(y; \mu, \sigma, \eta, \lambda) dy}{1 - F_{\text{Skt}}(0; \mu, \sigma, \eta, \lambda)} \\ &= \frac{F_{\text{Skt}}(h; \mu, \sigma, \eta, \lambda) - F_{\text{Skt}}(0; \mu, \sigma, \eta, \lambda)}{1 - F_{\text{Skt}}(0; \mu, \sigma, \eta, \lambda)}. \end{aligned} \quad (44)$$

The distribution function of the Exponential distribution is given by

$$F_{\text{Exp}}(h; \iota) = 1 - \exp\left(\frac{-h}{\iota}\right). \quad (45)$$

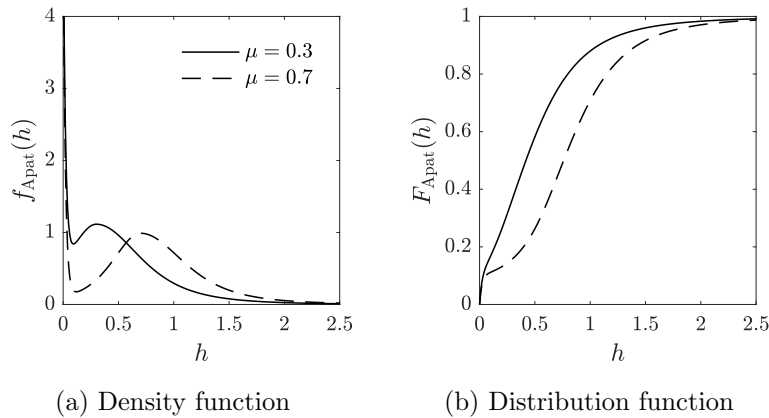


Figure 2: Plots of the density function $f_{\text{Apat}}(h; \mu, 0.6, 3, 0.2, 0.02, 0.9)$ and the distribution function $F_{\text{Apat}}(h; \mu, 0.6, 3, 0.2, 0.02, 0.9)$ of the Apatosaurus distribution for $\mu = 0.3$ (solid lines) and $\mu = 0.7$ (dashed lines).

Random number We can generate a random number h from an Apatosaurus distribution by first generating a component label l from a Bernoulli distribution with parameter w , and then generating $(h | l = 1) \sim F_{\text{TrSkt}}(h; \mu, \sigma, \eta, \lambda)$ or $(h | l = 0) \sim F_{\text{Exp}}(h; \iota)$. A truncated-skewed-t random number can be generated using the quantile function technique, by first generating u from an uniform distribution on the interval $(0, 1)$, and then applying the transformation $h = F_{\text{TrSkt}}^{-1}(u; \mu, \sigma, \eta, \lambda)$. We obtain the quantile function of the truncated-skewed-t distribution F_{TrSkt}^{-1} by inverting the distribution function in (44). Thus,

$$F_{\text{TrSkt}}^{-1}(u; \mu, \sigma, \eta, \lambda) = F_{\text{Skt}}^{-1}(u[1 - F_{\text{Skt}}(0; \mu, \sigma, \eta, \lambda)] + F_{\text{Skt}}(0; \mu, \sigma, \eta, \lambda); \mu, \sigma, \eta, \lambda), \quad (46)$$

where F_{Skt}^{-1} is the quantile function of the skewed-t distribution found by inverting the skewed-t distribution function in (31). Thus,

$$F_{\text{Skt}}^{-1}(u; \mu, \sigma, \eta, \lambda) = \begin{cases} \sigma(1 - \lambda) \sqrt{\frac{\eta - 2}{\eta}} F_{\text{St}, \eta}^{-1}\left(\frac{u}{1 - \lambda}\right) + \mu & \text{if } u < \frac{1 - \lambda}{2}, \\ \sigma(1 + \lambda) \sqrt{\frac{\eta - 2}{\eta}} F_{\text{St}, \eta}^{-1}\left(\frac{u}{1 + \lambda}\right) + \mu & \text{if } u \geq \frac{1 - \lambda}{2}, \end{cases} \quad (47)$$

where $F_{\text{St}, \eta}^{-1}$ is the quantile function of the Student t distribution with η degree-of-freedom. An Exponential random number can be generated in a similar fashion by transforming an uniform random number on $(0, 1)$ using the Exponential quantile function F_{Exp}^{-1} given by

$$F_{\text{Exp}}^{-1}(u; \iota) = -\iota \log(1 - u). \quad (48)$$

2.5.3 Conditional distribution of h_t

Employing the Apatosaurus distribution family developed in section 2.5.2, we model the conditional marginal distribution $F_{4,t}$, which correspond to the tail shape parameter h_t , as follows.

$$\begin{aligned} \xi_{4,t} &\sim F_{\text{Apat}}(\cdot; \mu_t, \sigma, \eta_4, \lambda_4, \iota, w_t), \\ \mu_t &= \delta_4 + \psi_4 \xi_{4,t-1} + \phi_4 \mu_{t-1}, \\ w_t &= 0.5 + 0.5 / \{1 + \exp[-\gamma(\mu_t - c)]\}, \\ \gamma &= \exp(\gamma^*). \end{aligned} \quad (49)$$

We assume that h_t follows an Apatosaurus distribution with time varying location and mixing weight parameters. Here the location parameter, μ_t , is the *mode* of the distribution, whose dynamics is given by the extended form of exponential smoothing. The conditional weight w_t is linked to μ_t via a logistic function, parametrised by $\gamma > 0$ and $c \in [0, 1]$, where γ controls how sensitive w_t is to the changes in μ_t , and c determines the location at which w_t is most sensitive to μ_t . This logistic link function allows the conditional distribution of h_t to shift more density to $h_t = 0$ for periods μ_t is closer to zero. It also restricts w_t to lie inside $[0.5, 1]$, so that the truncated-skewed-t component stays dominant. The mean of the conditional marginal distribution $\mathbb{E}(\xi_{4,t} | \mathcal{F}_{t-1})$ can be calculated using equation (42). The conditions $\delta_4 > 0$, $\psi_4 \geq 0$, $\phi_4 \geq 0$, and $\psi_4 + \phi_4 < 1$ are sufficient to ensure that μ_t is

positive and non-divergent.

3 Bayesian inference of DQF models

3.1 Likelihood and prior

As we now have a generative model for a quantile-function-valued time series, following from (24), the likelihood function of the gh-DQF model, denoted by f , can be written as

$$f(\boldsymbol{\xi}_1, \dots, \boldsymbol{\xi}_n; \boldsymbol{\theta}) = \prod_{t=1}^T f_t(\boldsymbol{\xi}_t; \boldsymbol{\theta}), \quad (50)$$

where $\boldsymbol{\theta}$ is the vector of model parameters. Let $\boldsymbol{\theta}_{i \in \{1,2,3\}} = (\delta_i, \psi_i, \phi_i, \omega_i, \alpha_i, \beta_i, \eta_i, \lambda_i)$, $\boldsymbol{\theta}_4 = (\delta_4, \psi_4, \phi_4, \gamma^*, c, \sigma, \eta_4, \lambda_4, \iota)$, and $\boldsymbol{\theta}_c = (\text{vech}(\mathbf{R})^\top, \nu)$, then $\boldsymbol{\theta} = (\boldsymbol{\theta}_1, \dots, \boldsymbol{\theta}_4, \boldsymbol{\theta}_c)$. An improper prior is used for $\boldsymbol{\theta}$ over the allowable parameter region. Let the indicator function I take the value one if $\boldsymbol{\theta}$ is in the allowable region and zero otherwise. Specifically,

$$I(\boldsymbol{\theta}) = \begin{cases} 1, & \text{if } \boldsymbol{\theta} \in \mathbb{A} = \bigcap_{i=1}^4 \mathcal{A}_i \\ 0, & \text{otherwise,} \end{cases} \quad (51)$$

where

$$\mathcal{A}_i = \left\{ \boldsymbol{\theta} \left| \begin{array}{l} -1 < \psi_i + \phi_i < 1, \\ \omega_i > 0, \alpha_i \geq 0, \beta_i \geq 0, \alpha_i + \beta_i < 1, \\ 2 < \eta_i \leq 40, -1 < \lambda_i < 1, \\ \delta_4 \geq 0, \psi_4 \geq 0, \phi_4 \geq 0, \\ -6 \leq \gamma^* \leq 6, 0 \leq c \leq 1, \\ \text{vech}(\mathbf{R}) \in [0, 1]^6, \min\{\text{eig}(\mathbf{R})\} > 0, \\ 2 < \nu \leq 40 \end{array} \right. \right\}. \quad (52)$$

The constraints on $\boldsymbol{\theta}_c$ and \mathbf{R} ensure that \mathbf{R} is a valid correlation matrix. The prior density, denoted by p , can be written as

$$\boldsymbol{\theta} \sim p(\boldsymbol{\theta}) \propto I(\boldsymbol{\theta}) \prod_{i=1}^3 \omega_i^{-1} \prod_{i=1}^4 \eta_i^{-2} \left[1 + \left(\frac{\iota}{10^{-5}} \right)^2 \right]^{-1} \nu^{-2}. \quad (53)$$

This prior is flat on most elements of $\boldsymbol{\theta}$ in \mathbb{A} with the exceptions of $\omega_1, \dots, \omega_3, \eta_1, \dots, \eta_4, \iota$, and ν . The marginal prior for ω_i reduces the upward bias typically observed for this intercept parameter in the conditional variance equation. The marginal prior for η_i behaves similar to a half-Cauchy prior, and is obtained by being flat on η_i^{-1} . Bauwens and Lubrano (1998) shows, using simulation, that the half-Cauchy prior results in a posterior mean closer to the true value than that obtained from an uniform prior. The marginal prior for ι is a half-Cauchy whose scale is 10^{-5} . For identifiability purpose, it is important to keep the mean parameter of the Exponential component of the Apatosaurus distribution close to zero. Finally, the marginal prior for ν is the same as that for η_i . With the likelihood

and prior defined, the kernel of the posterior density, denoted by π , can be computed as

$$\boldsymbol{\theta} \mid \boldsymbol{\xi}_1, \dots, \boldsymbol{\xi}_n \sim \pi(\boldsymbol{\theta}) \propto f(\boldsymbol{\xi}_1, \dots, \boldsymbol{\xi}_n; \boldsymbol{\theta}) p(\boldsymbol{\theta}). \quad (54)$$

3.2 Adaptive MCMC algorithm

In order to evaluate the various integrals of interest involving the posterior density given by (54), we generate a sample of points from the posterior distribution using an adaptive Markov Chain Monte Carlo (MCMC) algorithm. We first describe the sampling scheme in general, and then discuss the specific steps aimed at improving the mixing of the Markov chain.

One approach is to use a symmetric random-walk Metropolis (RWM) algorithm where we generate the entire parameter vector $\boldsymbol{\theta}$ simultaneously from a symmetric proposal distribution whose number of dimensions is equal to that of $\boldsymbol{\theta}$, and accept the move with the usual Metropolis acceptance probability. However, as $\boldsymbol{\theta}$ has 40 dimensions in our case, it may be difficult to tune the proposal distribution to achieve a satisfactory level of mixing. To mitigate this problem, we employ the well known strategy of updating the parameter vector in blocks, where a 40-dimensional move is broken into lower dimensional sub-moves. The blocking strategy is known to work well if the dependencies between the parameters in different blocks are low. Our model specification given by (23), (26), and (49) offers a somewhat natural partition of parameters. Let $\boldsymbol{\theta}_{[i]}$ denote the vector of parameters allocated to the i -th block. The entire parameter vector is then partitioned into ten blocks $\boldsymbol{\theta} = (\boldsymbol{\theta}_{[1]}, \dots, \boldsymbol{\theta}_{[10]})$. The specific blocking scheme is in Appendix A. Let $\cdot^{(j)}$ denote any vector or scalar associated with the state of the Markov chain in period j . We then move from $\boldsymbol{\theta}^{(j)}$ to $\boldsymbol{\theta}^{(j+1)}$ according to the following scheme.

- 1: **for** $i \leftarrow 1 : 10$ **do**
- 2: Generate $\boldsymbol{\theta}_{[i]}^{(j+1)} \mid \boldsymbol{\theta}_{[1]}^{(j+1)}, \dots, \boldsymbol{\theta}_{[i-1]}^{(j+1)}, \boldsymbol{\theta}_{[i+1]}^{(j)}, \dots, \boldsymbol{\theta}_{[10]}^{(j)}$.
- 3: **end for**

Thus, a single sweep of the entire parameter vector consists of ten sub-moves, where each sub-move or block is generated by a Metropolis step.

We generate a block-wise proposal for each $\boldsymbol{\theta}_{[i]}$, denoted by $\boldsymbol{\theta}_{[i]}^{(p)}$ from a symmetric proposal distribution with density $q_{[i]}$, and accept the proposal with the usual Metropolis acceptance probability given by

$$\min \left\{ \frac{\pi(\boldsymbol{\theta}^{(p)})}{\pi(\boldsymbol{\theta}^{(j)})}, 1 \right\}, \quad (55)$$

where

$$\boldsymbol{\theta}^{(p)} = (\boldsymbol{\theta}_{[1]}^{(j)}, \dots, \boldsymbol{\theta}_{[i-1]}^{(j)}, \boldsymbol{\theta}_{[i]}^{(p)}, \boldsymbol{\theta}_{[i+1]}^{(j)}, \dots, \boldsymbol{\theta}_{[10]}^{(j)}).$$

We choose the proposal density $q_{[i]}$ to be a mixture of multivariate normals with a different scale for each component,

$$q_{[i]} = \sum_{j=1}^{n_{\text{mix}}} w_j f_{\text{mvn}} \left(\cdot; \boldsymbol{\theta}_{[i]}^{(j)}, \Delta_{[i]}^2 s_j \boldsymbol{\Sigma}_{[i]} \right), \quad (56)$$

where s_j is the scale chosen for component j , and $\Delta_{[i]}$ is a tuning scale common to all components. Thus, all components are centred at $\theta_{[i]}^{(j)}$, with covariance structures differed only by scale. We heuristically choose the vector of mixing weights $\mathbf{w} = (w_1, w_2, w_3)$ to be $(0.7, 0.15, 0.15)$ and the corresponding vector of component scales $\mathbf{s} = (s_1, s_2, s_3)$ to be $(1, 100, 0.01)$. The intuition is that mixing relatively large jumps with relatively small ones would lower the chance of the chain getting “stuck”, either all together or in some dimensions of the parameter space.

With \mathbf{w} and \mathbf{s} chosen a priori, and a fixed covariance matrix $\Sigma_{[i]}$, the scale $\Delta_{[i]}$ is tuned automatically for each block during a tuning *epoch*. For a given $\Sigma_{[i]}$, we update the value of $\Delta_{[i]}$ every n_Δ iterations of the chain to target a specific acceptance rate, denoted by $r_{[i]}^{(\text{tar})}$. Let n_{epo} denote the number of iterations spent in a tuning epoch, and let $k \in \{n_\Delta(1, \dots, \lfloor \frac{n_{\text{epo}}-1}{n_\Delta} \rfloor)\}$ denote the iteration where a scale-update occurs. The new value of $\Delta_{[i]}$ is then given by

$$\Delta_{[i]}^{(k+1, \dots, k+n_\Delta)} = \Upsilon(r_{[i]}^{(\text{obs})}; r_{[i]}^{(\text{tar})}) \Delta_{[i]}^{(k-n_\Delta+1, \dots, k)}, \quad (57)$$

where Υ is a sensibly chosen tuning function that takes as an argument the realised acceptance rate since the last update, denoted by $r_{[i]}^{(\text{obs})}$. We choose Υ to be

$$\Upsilon(r_{[i]}^{(\text{obs})}; r_{[i]}^{(\text{tar})}) = \frac{\Phi^{-1}(r_{[i]}^{(\text{tar})}/2)}{\Phi^{-1}(r_{[i]}^{(\text{obs})}/2)}, \quad (58)$$

Although not strictly necessary, this particular tuning function explores the relationship between the scale of the proposal distribution Δ and the acceptance rate of the RWM algorithm r when both the proposal and target distributions are d -dimensional normal (Roberts and Rosenthal, 2001); $r = 2\Phi(-\Delta\sqrt{d}/2)$. Even if this relationship does not strictly hold in practice, as Υ is both positive and monotonically increasing on the interval $(0, 1)$ while being equal to one for $r_{[i]}^{(\text{obs})} = r_{[i]}^{(\text{tar})}$, the tuning function in (58) will still behave sensibly. We set the target acceptance rate according to the size of the block $d_{[i]}$ by following the empirically successful heuristics based on the results of Gelman et al. (1996). Specifically, we choose $r_{[i]}^{(\text{tar})} = 0.44$ for $d_{[i]} = 1$, $r_{[i]}^{(\text{tar})} = 0.35$ for $2 \leq d_{[i]} \leq 4$, and $r_{[i]}^{(\text{tar})} = 0.234$ for $d_{[i]} > 4$. The initial scale of each block $\Delta_{[i]}^{(1, \dots, n_\Delta)}$ is set to $2.38/\sqrt{d_{[i]}}$.

We gradually improve the estimate of the covariance matrix of the proposal distribution for each block $\Sigma_{[i]}$ by running multiple tuning epochs. With the exception of the first epoch, we initialise the chain of each epoch with the last generated parameter vector of the previous epoch, and set the covariance matrix of each block to the sample covariance matrix of the corresponding block of the previous epoch. A few initial iterations of each epoch is discarded when computing the sample covariance matrix; we denote this number by $n_{\text{disc}}^{(\text{epo})}$. The number of tuning epochs required is judged by a simple stopping criterion based on the mean absolute percentage change (MAPC) given by

$$\text{MAPC}_j = \frac{1}{40} \sum_{i=1}^{40} \left| \frac{\hat{\sigma}_{\theta,i}^{(j)} - \hat{\sigma}_{\theta,i}^{(j-1)}}{\hat{\sigma}_{\theta,i}^{(j-1)}} \right|, \quad (59)$$

where $\hat{\sigma}_{\theta,i}^{(j)}$ denotes the sample standard deviation of the i -th dimension of the chain from the j -th epoch. Adaptation is stopped after j epochs if $j_{\min} \leq j \leq j_{\max}$ and $\text{MAPC}_j \leq \varepsilon_{\text{mapc}}$, where j_{\min} and j_{\max} are the least and most number of tuning epochs, and $\varepsilon_{\text{mapc}}$ is a tolerance level. In all the applications, we set $j_{\min} = 2$, $j_{\max} = 30$, $\varepsilon_{\text{mapc}} = 0.1$, $n_{\text{epo}} = 12000$, and $n_{\text{disc}}^{(\text{epo})} = 2000$. Note that any convergence criterion can be used to terminate the adaptation, however we find the MAPC to be effective in practice while having the advantage of being computationally simple.

Once the adaptive phase ends, the RWM sampler transitions into the sampling phase where all adaptations are tuned-off. That is, we generate a Markov chain according to our sampling scheme with $\Delta_{[i]}$ and $\Sigma_{[i]}$ fixed. The scale $\Delta_{[i]}$ and covariance matrix $\Sigma_{[i]}$ are fixed at, respectively, the mean of the tuned scales and the sample covariance matrix of the generated parameters, over the iterations of the final tuning epoch after discarding the first $n_{\text{disc}}^{(\text{epo})}$ ones. The sample mean of the generated parameters over these iterations is used as the initial state of the sampling phase chain.

Notice that, in our sampling scheme, the posterior kernel in (54) must be evaluated at least once when computing the acceptance probability in (55) for each block update. Naively evaluating the entire posterior kernel for each sub-move can be computationally costly. However, because of the way in which the blocks are chosen and the special structure of the conditional joint density of ξ_t in (24), computational cost can be reduced substantially by only updating the part of the likelihood related to each sub-move. For example, the vectors $(f_{1,1}(\xi_{1,1}), \dots, f_{1,T}(\xi_{1,T}))$, $(u_{1,1}, \dots, u_{1,T}) = (F_{1,1}(\xi_{1,1}), \dots, F_{1,T}(\xi_{1,T}))$, and $(F_{\text{St}}^{-1}(u_{1,1}), \dots, F_{\text{St}}^{-1}(u_{1,T}))$ only need to be recomputed when updating the blocks $\theta_{[1]}^{(j+1)}$ and $\theta_{[2]}^{(j+1)}$.

4 Simulation study

A simulation study is conducted to investigate the effectiveness of the adaptive MCMC sampling algorithm proposed in Section 3.2. We generate 1000 independent datasets from the true data generating process (DGP), with each dataset containing 3000 observations. The true DGP is the model for the conditional joint distribution of ξ_t specified in Section 2.5 whose parameters values are chosen to be similar to the parameter estimates from the real data. The sampling phase of the MCMC algorithm is set to run for 105000 iterations. The posterior mean estimates of the parameters are computed using the last 100000 iterations from the sampling phase.

In Table 1, for each parameter, we report the true parameter value (True), Monte Carlo (MC) mean of the 1000 posterior mean estimates (Mean), and 95% MC interval (Lower, Upper). The posterior mean estimates are all reasonably close to the true values, with all the MC intervals covering the true values.

θ_1	δ_1	ψ_1	ϕ_1	ω_1	α_1	β_1	η_1	λ_1	
True	0.000	0.060	0.910	6.000E-08	0.150	0.840	8.000	-0.160	
Mean	1.914E-07	0.062	0.902	6.679E-08	0.151	0.837	8.244	-0.161	
Lower	-4.714E-06	0.048	0.869	4.440E-08	0.125	0.807	6.512	-0.206	
Upper	5.330E-06	0.078	0.925	9.616E-08	0.180	0.863	10.991	-0.114	
θ_2	δ_2	ψ_2	ϕ_2	ω_2	α_2	β_2	η_2	λ_2	
True	-0.130	0.430	0.530	5.000E-03	0.060	0.880	15.000	0.000	
Mean	-0.135	0.432	0.527	5.981E-03	0.064	0.865	15.410	0.011	
Lower	-0.168	0.405	0.500	3.230E-03	0.043	0.799	10.300	-0.038	
Upper	-0.106	0.456	0.556	1.039E-02	0.087	0.912	24.104	0.057	
θ_3	δ_3	ψ_3	ϕ_3	ω_3	α_3	β_3	η_3	λ_3	
True	0.000	0.050	0.930	7.000E-05	0.070	0.920	18.000	0.140	
Mean	-9.664E-06	0.053	0.921	8.360E-05	0.073	0.915	19.011	0.138	
Lower	-2.251E-04	0.040	0.894	4.428E-05	0.055	0.893	11.922	0.089	
Upper	2.197E-04	0.069	0.942	1.466E-04	0.092	0.937	28.197	0.187	
θ_4	δ_4	ψ_4	ϕ_4	γ^*	c	σ	η_4	λ_4	ι
True	3.000E-03	0.220	0.740	3.700	0.030	0.060	6.000	0.150	1.000E-04
Mean	3.804E-03	0.218	0.737	3.689	0.031	0.060	6.100	0.151	8.164E-05
Lower	2.063E-03	0.199	0.712	3.458	0.012	0.057	4.905	0.098	5.528E-05
Upper	5.906E-03	0.239	0.761	3.960	0.049	0.063	7.804	0.204	1.095E-04
θ_c	$\mathbf{R}_{2,1}$	$\mathbf{R}_{3,1}$	$\mathbf{R}_{4,1}$	$\mathbf{R}_{3,2}$	$\mathbf{R}_{4,2}$	$\mathbf{R}_{4,3}$	ν		
True	-0.300	-0.100	0.200	-0.220	-0.600	0.120	15.000		
Mean	-0.299	-0.099	0.193	-0.220	-0.580	0.115	14.583		
Lower	-0.331	-0.136	0.158	-0.257	-0.606	0.076	11.344		
Upper	-0.267	-0.062	0.227	-0.184	-0.553	0.152	19.737		

Table 1: True values and summary statistics for the posterior mean estimates of the DQF model parameters.

The MC mean of the acceptance rates for the last 10^4 iterations of the sampling phase is reported in Table 2 for each parameter block.

Block (Size)	1 (3)	2 (5)	3 (3)	4 (5)	5 (3)	6 (5)	7 (5)	8 (4)	9 (6)	10 (1)
Target	0.350	0.234	0.350	0.234	0.350	0.234	0.234	0.350	0.234	0.440
Mean	0.345	0.223	0.344	0.230	0.345	0.230	0.231	0.348	0.230	0.438

Table 2: Mean acceptance rate of each block during the sampling phase.

5 Empirical Studies

5.1 Cleaning of High Frequency Data

All of the following empirical studies rely on high-frequency price data of major international stock indices. As high-frequency intra-daily data are collected via real-time streaming of asynchronous messages, recording errors are present in the raw data. Furthermore, the raw data also contains artefacts due to events such as trading halts, lunch breaks, and special orders outside the normal trading hours. Therefore, it is important to pre-process

the raw data to remove as many incorrectly recorded prices as possible (Brownlees and Gallo, 2006).

For our empirical analysis, we use transaction prices sampled at one-minute intervals. The raw data is provided by the Thomson Reuters Tick History. Let $\zeta_t = (\zeta_{t,1}, \dots, \zeta_{t,n_t})$ denote the vector of intra-daily prices for day t . To clean the data, we apply the following set of rules for each t :

- I. For $i \in \{1, \dots, n_t\}$, remove $\zeta_{t,i}$ if its timestamp is outside the normal trading hours.
- II. For $i \in \{1, \dots, n_t\}$, remove $\zeta_{t,i}$ if $\zeta_{t,i} \leq 0$.
- III. For $j \in \{2, \dots, n_t\}$, remove $\zeta_{t,1}, \dots, \zeta_{t,j-1}$ if $\zeta_{t,1} = \dots = \zeta_{t,j}$.
- IV. For $j \in \{2, \dots, n_t\}$, remove $\zeta_{t,n_t-j+1}, \dots, \zeta_{t,n_t-1}$ if $\zeta_{t,n_t-j+1} = \dots = \zeta_{t,n_t}$.
- V. For $i \in \{1, \dots, n_t - j + 1\}$ and $j \in \{31, \dots, n_t\}$, remove $\zeta_{t,i}, \dots, \zeta_{t,i+j-2}$ if $\zeta_{t,i} = \dots = \zeta_{t,i+j-1}$.
- VI. For $i \in \{1, \dots, n_t\}$, remove $\zeta_{t,i}$ if its outlier score is greater than 20.
- VII. Remove $\zeta_{t,1}, \dots, \zeta_{t,n_t}$ if $n_t < 60$.

Note that the rules are applied in sequence. I.e., ζ_t and n_t are updated after each rule is applied. The difficulty in implementing rule I is that changes have been made over time to the normal trading hours for many major stock exchanges. Therefore, we must keep track of all the changes for each stock exchange over our sample period. A complete history of session times is documented in Appendix C. Rule II removes any obvious mistakes. Rules III and IV are responsible for removing static prices at the beginning and the end of a day, which usually indicate events such as late starts and trading halts. Similarly, rule V removes any static gaps that are longer than 30 minutes. For rule VI, an outlier score is computed for each $\zeta_{t,i}$, which is a scale-invariant distance measure between $\zeta_{t,i}$ and its neighbouring observations. See Appendix D for details on computing the outlier score. Finally, rule VII removes the entire trading day if there are less than 60 observations left after applying the first six rules.

Our data includes one-minute price series of ten major stock indices: S&P 500 (SPX), Dow Jones Industrial Average (DJIA), NASDAQ Composite (Nasdaq), FTSE 100 (FTSE), DAX, CAC 40 (CAC), Nikkei Stock Average 225 (Nikkei), Hang Seng (HSI), Shanghai Composite (SSEC), and All Ordinaries (AORD). The sample period starts on January 3, 1996 and ends on May 24, 2016. Table 3 shows the percentage proportion of removed observations after applying all the rules for each stock index. It also documents the number of trading days and the number of observations for each index before cleaning.

	Days	Obs.	Del. (%)
SPX	5103	1979767	0.12
DJIA	5105	1977270	0.02
Nasdaq	5112	1975540	0.17
FTSE	5380	2562661	0.23
DAX	5036	2470843	0.09
CAC	5167	2533410	0.17
Nikkei	4977	1345816	0.04
HSI	4998	1299330	0.01
SSEC	4906	1175712	0.05
AORD	5138	1779671	0.09

Table 3: Data cleaning summary

5.2 A Case Study of S&P 500 One-Minute Returns

In this part of the empirical study, the goal is demonstrate the various aspects of the DQF model by focusing on arguably one of the most widely followed market indices – the S&P 500. We dynamically model the daily distributions of one-minute percentage log-returns. For each trading day, there are approximately 390 one-minute returns. Let $\mathbf{y}_t = (y_{t,1}, \dots, y_{t,n_t})$ denote the one-minute returns for day t . For each $t \in \{1, \dots, T\}$, the return vector is computed by applying

$$y_{t,i} = 100 [\log(\zeta_{t,i+1}) - \log(\zeta_{t,i})],$$

for each $i \in \{1, \dots, n_t - 1\}$. We then summarise each \mathbf{y}_t by a QF-valued observation $X_t = S(\mathbf{y}_t)$. The symbol constructor S here corresponds to the L-moment estimator of g-and-h parameters.

To illustrate that the g-and-h quantile functions are adequate summaries of the distributional features of one-minute returns, QQ-plots are shown in Figure 3 where sample quantiles of one-minute returns are plotted against the estimated g-and-h quantiles for three stylised days. On the last trading day of a very volatile year, December 31, 2009, the returns are strongly negatively skewed. An infamous “flash crash” occurred on May 6, 2010, which resulted in one-minute returns being extremely heavy-tailed. On April 4, 2014, the intra-daily returns are approximately normally distributed. From the QQ-plots, it can be seen that the g-and-h quantile functions can provide reasonable approximations to these distributional shapes.

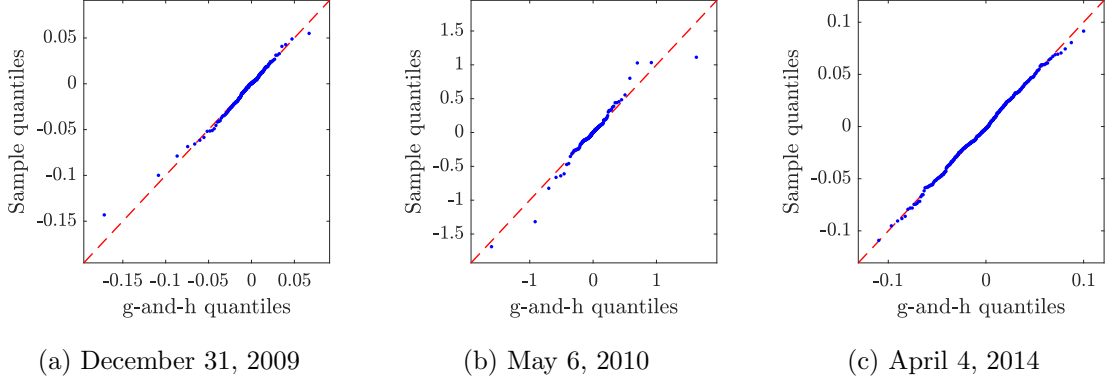


Figure 3: QQ-plots of one-minute returns of three specific trading days against g-and-h quantiles.

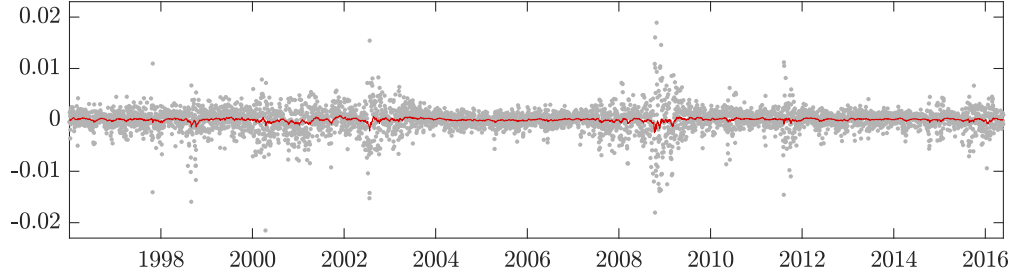
The four-dimensional mapped vector is finally obtained via $\boldsymbol{\xi}_t = \mathcal{M}(X_t)$ for each $t \in \{1, \dots, T\}$. The conditional joint distribution of $\boldsymbol{\xi}_t$ is given by the model in Section 2.5. The parameters are estimated using the adaptive MCMC algorithm described in Section 3.2 whose configuration is identical to that for the simulation study.

Summary statistics of the estimated posterior are reported in Tables 4. The parameters driving the conditional mean dynamics ψ_1, \dots, ψ_4 and ϕ_1, \dots, ϕ_4 are all estimated to be nonzero, as indicated by their credible intervals. The fact that the estimates of ψ_1 and ψ_3 are much closer to zero than those of ψ_2 and ψ_4 indicates that the observed values of a_t and g_t are much less informative than those of b_t^* and h_t about the respective conditional means at period $t + 1$. The estimates of the logistic link function parameters γ^* and c confirm that the Exponential component of the Apatosaurus distribution is only needed when h_t is small. The fact that the copula parameters $\mathbf{R}_{2,1}$ and $\mathbf{R}_{3,2}$ are both estimated to be negative suggests that an increase in volatility is more likely to be accompanied by negative returns. This observation is in accordance with the well-documented “leverage effect” observed in daily equity returns. However, it is surprising to observe a rather large negative estimate for $\mathbf{R}_{4,2}$, which suggests a negative relationship between volatility and tail index.

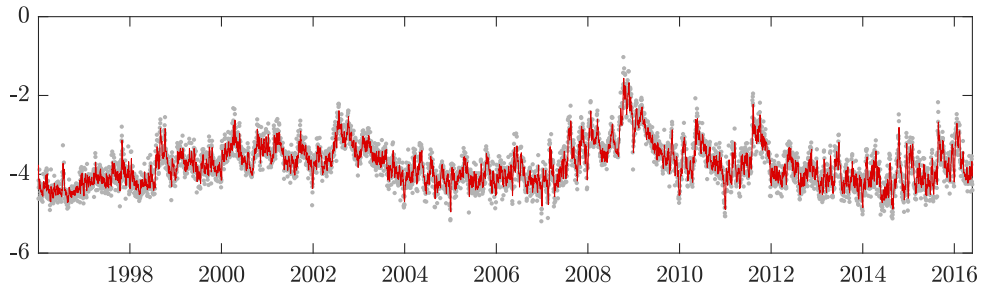
θ_1	δ_1	ψ_1	ϕ_1	ω_1	α_1	β_1	η_1	λ_1	
Mean	1.741E-06	0.034	0.924	6.492E-08	0.144	0.846	7.332	-0.162	
Lower	-1.248E-06	0.024	0.892	4.456E-08	0.120	0.820	6.097	-0.200	
Upper	5.369E-06	0.046	0.951	8.959E-08	0.170	0.870	8.943	-0.123	
θ_2	δ_2	ψ_2	ϕ_2	ω_2	α_2	β_2	η_2	λ_2	
Mean	-0.124	0.435	0.533	4.161E-03	0.047	0.890	21.702	0.059	
Lower	-0.149	0.411	0.505	2.209E-03	0.032	0.832	13.826	0.022	
Upper	-0.100	0.460	0.560	7.143E-03	0.066	0.931	34.779	0.096	
θ_3	δ_3	ψ_3	ϕ_3	ω_3	α_3	β_3	η_3	λ_3	
Mean	2.002E-04	0.023	0.932	1.982E-05	0.020	0.978	19.546	0.145	
Lower	9.734E-06	0.012	0.872	5.323E-10	0.013	0.967	13.028	0.089	
Upper	5.249E-04	0.035	0.970	5.366E-05	0.030	0.986	31.264	0.185	
θ_4	δ_4	ψ_4	ϕ_4	γ^*	c	σ	η_4	λ_4	ι
Mean	2.737E-03	0.193	0.773	3.743	0.014	0.061	6.815	0.134	6.337E-05
Lower	1.152E-03	0.175	0.749	3.569	0.001	0.059	5.569	0.087	4.109E-05
Upper	4.433E-03	0.212	0.796	3.956	0.032	0.063	8.507	0.181	9.450E-05
θ_c	$\mathbf{R}_{2,1}$	$\mathbf{R}_{3,1}$	$\mathbf{R}_{4,1}$	$\mathbf{R}_{3,2}$	$\mathbf{R}_{4,2}$	$\mathbf{R}_{4,3}$	ν		
Mean	-0.288	-0.065	0.176	-0.229	-0.524	0.086	20.120		
Lower	-0.315	-0.094	0.147	-0.256	-0.545	0.058	15.843		
Upper	-0.262	-0.037	0.203	-0.202	-0.503	0.114	26.117		

Table 4: DQF posterior summary for S&P 500, showing the posterior mean (Mean) and the 95% credible interval (Lower, Upper) for each parameter.

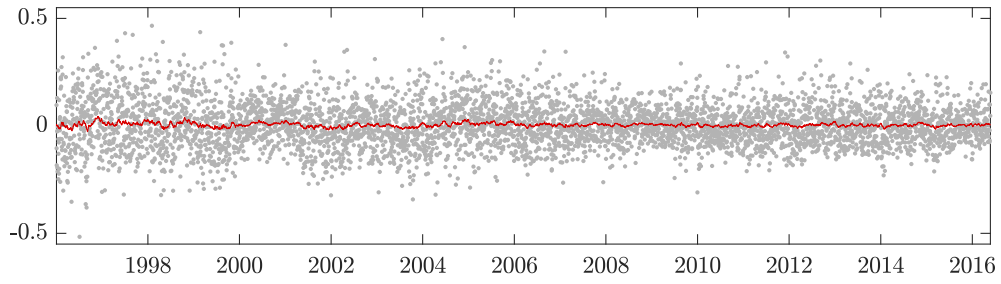
The posterior mean estimates of the conditional means $\{\mathbb{E}(\boldsymbol{\xi}_t | \mathcal{F}_{t-1})\}$ are plotted in Figure 4, together with the realised values of $\{\boldsymbol{\xi}_t\}$. Firstly, compared to $\{a_t\}$ and $\{g_t\}$, the unconditional variances of $\{b_t^*\}$ and $\{h_t\}$ appear to be much better explained by the variations in the conditional means. As expected, the values of h_t are clearly above zero for most of the days, indicating that one-minute returns are heavy-tailed. Finally, the negative relationship between b_t^* and h_t is apparent in sub-plots (b) and (d); during high volatility periods, h_t can become vary close to zero.



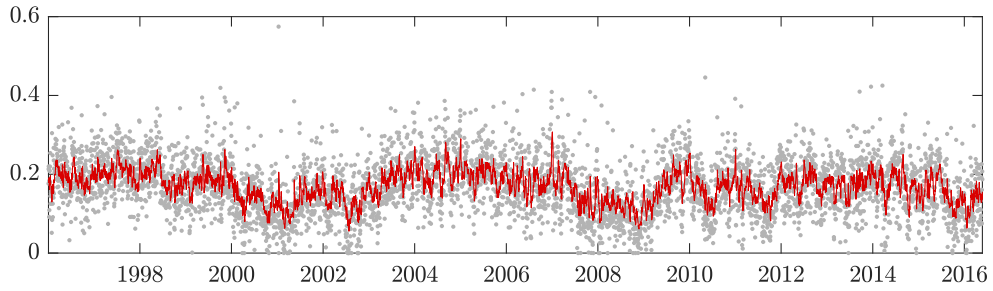
(a) a_t



(b) b_t^*



(c) g_t



(d) h_t

Figure 4: Posterior mean estimates of $\{\mathbb{E}(\xi_t | \mathcal{F}_{t-1})\}$ (red line) plotted over $\{\xi_t\}$ (grey dots).

Recall that the filtered quantile function (i.e., one-step-ahead forecast) can be obtained from the conditional mean of ξ_t by applying the inverse mapping

$$\tilde{X}_t = \mathcal{M}^{-1}(\mathbb{E}[\xi_t | \mathcal{F}_{t-1}]).$$

To illustrate, in Figure 5, we plot $\tilde{X}_1(u), \dots, \tilde{X}_T(u)$ at various values of u . Notice that evaluating \tilde{X}_t at multiple quantile levels does not require multiple estimations of the DQF model, and the quantile estimates do not cross over time.

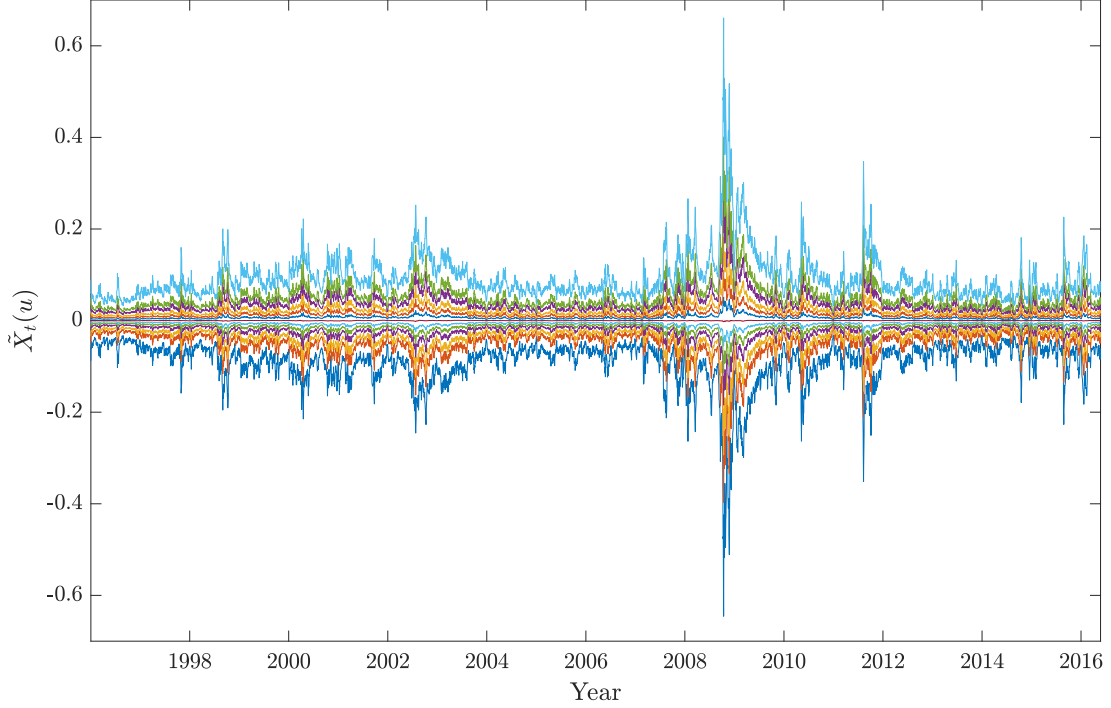


Figure 5: Posterior mean estimates of $\{\tilde{X}_t(u)\}$ for $u \in \{0.01, 0.05, 0.25, 0.5, 0.75, 0.95, 0.99\}$.

A considerable amount of effort is spent on constructing the conditionally Apatosaurus marginal model with time-varying weights for $\{h_t\}$. The posterior mean estimates of the conditional weights are plotted in Figure 6, together with the realised $\{h_t\}$. As expected, the weights are close to one for most of the days; the Exponential component only plays a role for when h_t is close to zero. As the weights are closed to one on average, it is worth knowing whether an advantage is gained over a simpler truncated-skewed-t alternative. To see this, we estimate a truncated-skewed-t model $h_t \sim F_{\text{TrSkt}}(\cdot; \mu_t, \sigma, \eta, \lambda)$, where $\mu_t = \delta + \psi h_{t-1} + \phi \mu_{t-1}$. Let $u_{\text{TrSkt},t} = F_{\text{TrSkt}}(h_t; \hat{\mu}_t, \hat{\sigma}, \hat{\eta}, \hat{\lambda})$ be the probability integral transform (PIT) of h_t , where $\hat{\mu}_t, \hat{\sigma}, \hat{\eta}$, and $\hat{\lambda}$ are the posterior mean estimates. If the truncated-skewed-t model is adequate, $Z(u_{\text{TrSkt},t})$ will be a draw from the standard normal distribution, where Z denotes the standard normal quantile function. Similarly, let $u_{\text{Apat},t}$ denote the PIT of h_t under the Apatosaurus model given by (49) where the posterior mean estimates are also used for the time-varying and constant parameters. We plot both $\{Z(u_{\text{TrSkt},t})\}$ and $\{Z(u_{\text{Apat},t})\}$ against the standard normal quantiles in Figure 7. It is apparent that without the added Exponential component, the truncated-skewed-t

model is not flexible enough for the left tail of the $\{h_t\}$.

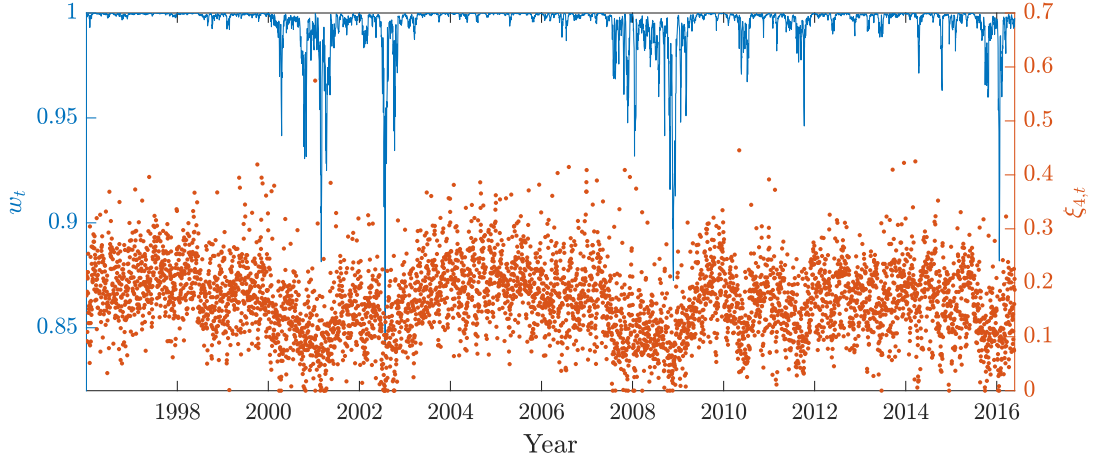


Figure 6: Posterior mean estimates of $\{w_t\}$ (blue line, left axis) plotted together with $\{h_t\}$ (orange dots, right axis).

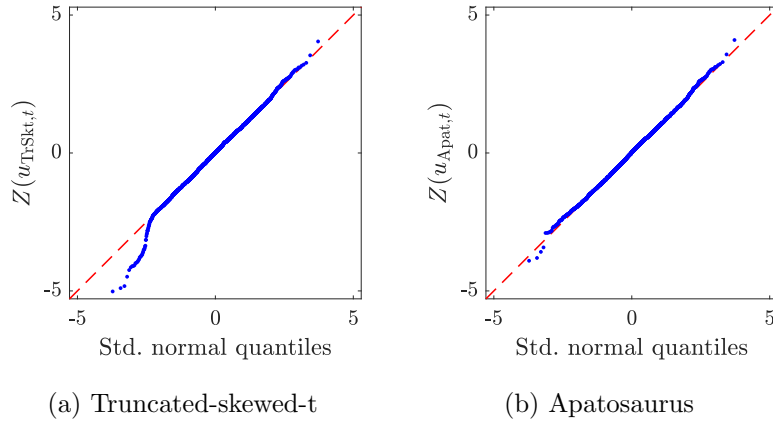


Figure 7: QQ-plots of transformed $\{h_t\}$ under truncated-skewed-t and Apatosaurus models against standard normal quantiles.

5.3 An Investigation into Time Series Informativeness

One advantage of our approach is that it enables us to separately study the time series predictability of various characteristics of intra-daily return distributions. By examining the plots in Figure 4 and the parameter estimates of ψ_1, \dots, ψ_4 and ϕ_1, \dots, ϕ_4 , it seems apparent that some marginal processes are more “informative” than others. For example, it seems reasonable to state that the time series of b_t^* and h_t appear to be more predictable than those of a_t and g_t . Here we formally quantify such informativeness in time series, by proposing a model based measure, called *signal ratio*. Let $\{\xi_t: t \in \mathbb{Z}\}$ be a real-valued covariance stationary process. The signal ratio, denoted by R_{Sig} , is then defined as

$$R_{\text{Sig}} = \frac{\text{Var}[\mathbb{E}(\xi_t | \mathcal{F}_{t-1})]}{\text{Var}(\xi_t)},$$

where $\mathcal{F}_{t-1} = \sigma(\{\xi_s: s \leq t-1\})$ is the natural filtration. Intuitively, R_{Sig} measures the proportion of unconditional variance explained by the variation in conditional means. The signal ratio nomenclature derives from the interpretation of conditional means as unobserved signals of a noisy process. It is easily checked that an i.i.d. process has a signal ratio of zero, while a fully deterministic process has a signal ratio of one. The expression of R_{Sig} is available in closed form for the marginal model for $\{a_t\}$, $\{b_t^*\}$, and $\{g_t\}$. It can be computed numerically using simulation for the Apatosaurus model for $\{h_t\}$. Additional material on signal ratio is given in Appendix B. The posterior mean estimates of R_{Sig} and 95% credible intervals are plotted in Figure 8 for each margin. The R_{Sig} estimates are consistently high for $\{b_t^*\}$ across all indices, which justifies models that make use of realised measures of dispersion. For $\{h_t\}$, the estimates vary considerably across indices, with Nikkei being the highest and SSEC being the lowest; for some indices, the posteriors are much more diffused compared to those for $\{b_t^*\}$. All the R_{Sig} estimates for $\{a_t\}$ and $\{g_t\}$ are close to zero, except perhaps for SSEC, which suggests that it is in general difficult to predict the location and asymmetry of one-minute returns.

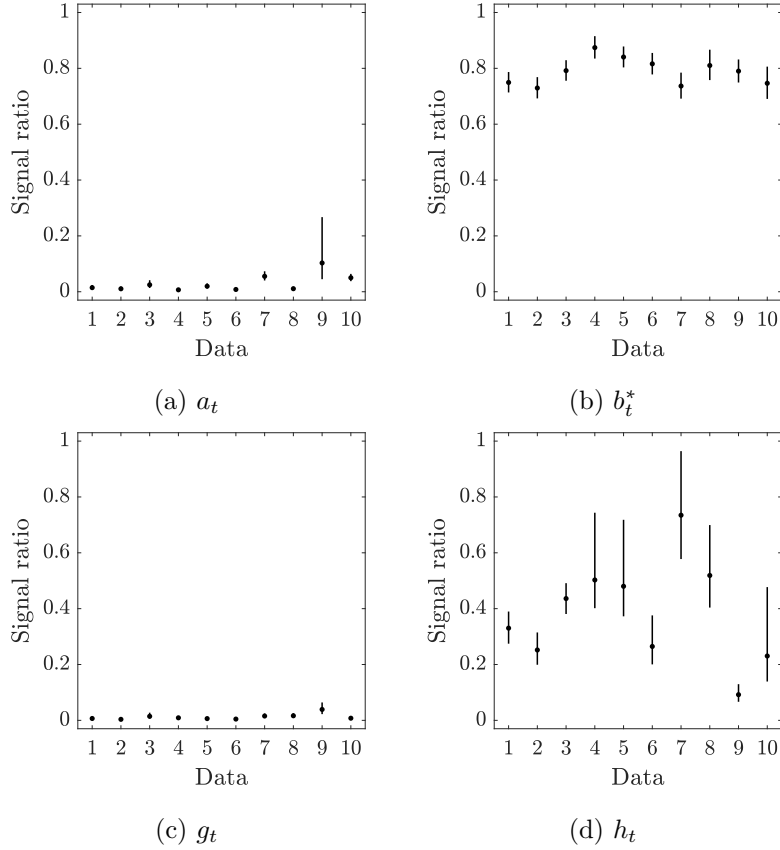


Figure 8: Posterior mean estimates (dots) and credible intervals (bars) of signal ratios for each marginal model. The numbers $1, \dots, 10$ are used to identify the ten indices: 1–SPX, 2–DJIA, 3–Nasdaq, 4–FTSE, 5–DAX, 6–CAC, 7–Nikkei, 8–HSI, 9–SSEC, 10–AORD.

5.4 Value-at-Risk of Daily Returns via Quantile Scaling

Value-at-Risk (VaR) is a risk measure used by financial institutions world wide, and is defined as a quantile of a return distribution. Being able to accurately forecast VaR of daily asset returns is crucial for risk management. In this subsection, we demonstrate that one can indeed compute dynamically the VaR of daily returns using the output of the DQF model, using a method called quantile scaling.

Let $q_{u,t}^M$ and $q_{u,t}^D$ be the u -level quantiles of one-minute and daily returns, respectively. Let $\mathbf{y}^D = (y_1^D, \dots, y_T^D)$ be a sequence of daily close-to-close returns. We assume there exists a scaling factor s_u , such that

$$q_{u,t}^D = s_u q_{u,t}^M. \quad (60)$$

As the DQF model gives us an estimate of the u -level quantile of one-minute returns for each day, we can let $q_{u,t}^M = \tilde{X}_t(u)$. The estimate of the scaling factor \hat{s}_u can be found by solving the quantile regression minimisation problem (Koenker and Bassett, 1978)

$$\hat{s}_u = \arg \min_{s_u} \sum_{t=1}^T \rho_u(y_t^D - s_u q_{u,t}^M), \quad (61)$$

where the loss function ρ_u is defined by

$$\rho_u(\varepsilon) = \varepsilon[u - I_{\{\varepsilon < 0\}}(\varepsilon)]. \quad (62)$$

It is shown by Yu and Moyeed (2001) that minimising the objective function in (61) is numerically equivalent to maximising a likelihood function where the observations are assumed to follow the asymmetric Laplace (AL) distributions. The AL family has the following density function

$$f_{AL}(\varepsilon; \mu, \sigma, u) = \frac{u(1-u)}{\sigma} \exp\left[-\rho_u\left(\frac{\varepsilon - \mu}{\sigma}\right)\right], \quad (63)$$

where $\mu \in \mathbb{R}$, $\sigma \in (0, \infty)$, and $u \in (0, 1)$ are the location, scale, and asymmetry parameters, respectively.

When y_t^D is assumed to follow an AL distribution with the location parameter being $s_u q_{u,t}^M$, the likelihood function is then given by

$$\begin{aligned} f(\mathbf{y}^D; s_u, \sigma) &= \prod_{t=1}^T f_{AL}(y_t^D; s_u q_{u,t}^M, \sigma, u) \\ &\propto \sigma^{-T} \exp\left[-\sigma^{-1} \sum_{t=1}^T \rho_u(y_t^D - s_u q_{u,t}^M)\right]. \end{aligned} \quad (64)$$

The prior density p is then defined by placing an improper flat prior on s_u and an inverse prior on σ ,

$$s_u, \sigma \sim p(s_u, \sigma) \propto \sigma^{-1}. \quad (65)$$

The posterior density π is then given by

$$\begin{aligned} s_u, \sigma \mid \mathbf{y}^D &\sim \pi(s_u, \sigma) \propto f(\mathbf{r}^D; s_u, \sigma) p(s_u, \sigma) \\ &\propto \sigma^{-(T+1)} \exp \left[-\sigma^{-1} \sum_{t=1}^T \rho_u(y_t^D - s_u q_{u,t}^M) \right]. \end{aligned} \quad (66)$$

As we are only interested in the scaling factor s_u , we integrate out the scale parameter σ to obtain the marginal posterior density of s_u . Using the fact that (66) has the form of the kernel of an Inverse Gamma density in σ , and that a density function must integrate to one, the marginal posterior of s_u can be obtained in closed-form (Gerlach et al., 2011);

$$\int_0^\infty \pi(s_u, \sigma) d\sigma = \left[\sum_{t=1}^T \rho_u(y_t^D - s_u q_{u,t}^M) \right]^{-T}. \quad (67)$$

To compute the VaR estimates of daily returns at quantile level u , we first sample from the univariate posterior in (67) using the adaptive MCMC sampler described in Section 3.2, where we plug-in the posterior mean estimates of $\{\tilde{X}_t(u)\}$ for $\{q_{u,t}^M\}$. Of course, only a single block is needed here. The posterior distribution of $q_{u,t}^D$ conditional on $\{q_{u,t}^M\}$ is then approximated via the posterior draws for s_u .

5.5 Forecasting Value-at-Risk

In this final part of the empirical studies, the DQF model is applied to forecast one-day-ahead the VaR of daily returns, for quantile levels 0.05 and 0.01. The quantile scaling method described in Section 5.4 is employed to generate the daily scale forecasts.

Posterior mean estimates of one-day-ahead forecasts are computed for $t \in \{3001, \dots, T\}$ using the most updated posterior sample. The adaptive MCMC algorithm is run every 10 days to update the posterior sample, at estimation point $t_E \in \{3000, 3010, \dots\}$ using the past 3000 QF-valued observations $\{X_{t_E-3000+1}, \dots, X_{t_E}\}$. The one-day-ahead out-of-sample VaR forecasts are plotted over daily returns for S&P 500 and FTSE in Figures 9 and 10, respectively. The posterior mean estimates of the scaling factors used for VaR forecasts are plotted in Figures 11 and 12 for S&P 500 and FTSE, respectively.

As VaR is an *elicitable* risk measure (Gneiting, 2011), the following scoring function is used to rank VaR forecasts from competing models.

$$\mathcal{S}_u(q, y) = (I_{\{y \leq q\}} - u)(y - q). \quad (68)$$

It can be shown that $q_{u,t}^D$ minimises $\mathbb{E}[\mathcal{S}_u(q_{u,t}^D, y^D) \mid \mathcal{F}_{t-1}]$ if $q_{u,t}^D$ is the u -level quantile of the conditional distribution of y_t^D (McNeil et al., 2015). The competing models are CAViaR-SAV, GJR-GARCH with t distribution (GJR-t), GJR-GARCH with skewed- t distribution (GJR-skt), Realized-GARCH with t distribution (Realized-t), and Realized-GARCH with skewed- t distribution (Realized-skt). The value of the scoring function in (68) is computed for each day of the forecast period. For each model, the sample mean of the scoring function is reported in Table 5. It is encouraging to see that the DQF model minimises the mean scoring function in each case.

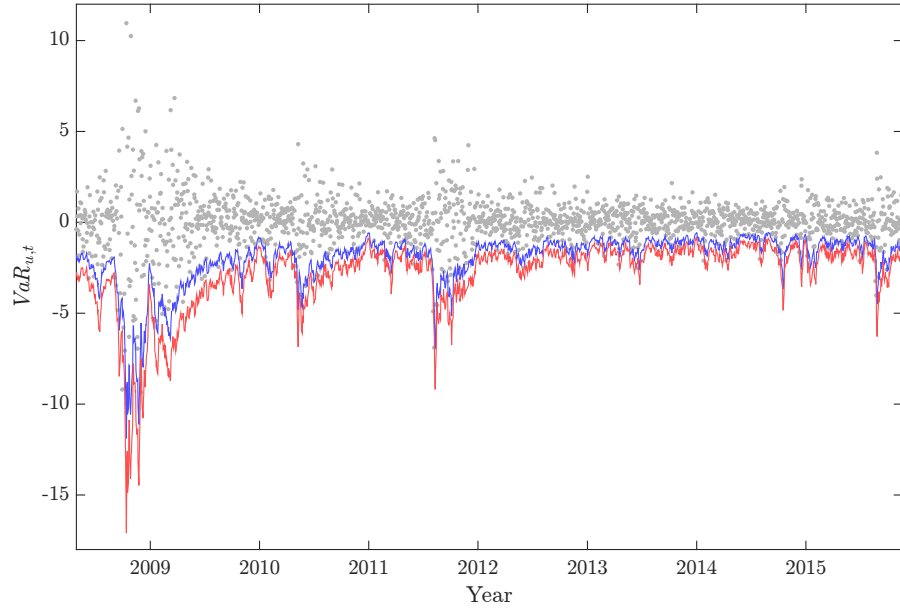


Figure 9: One-step-ahead forecasts of $VaR_{u,t}$ for $u \in \{0.01, 0.05\}$ given by the posterior mean for the S&P 500 index.

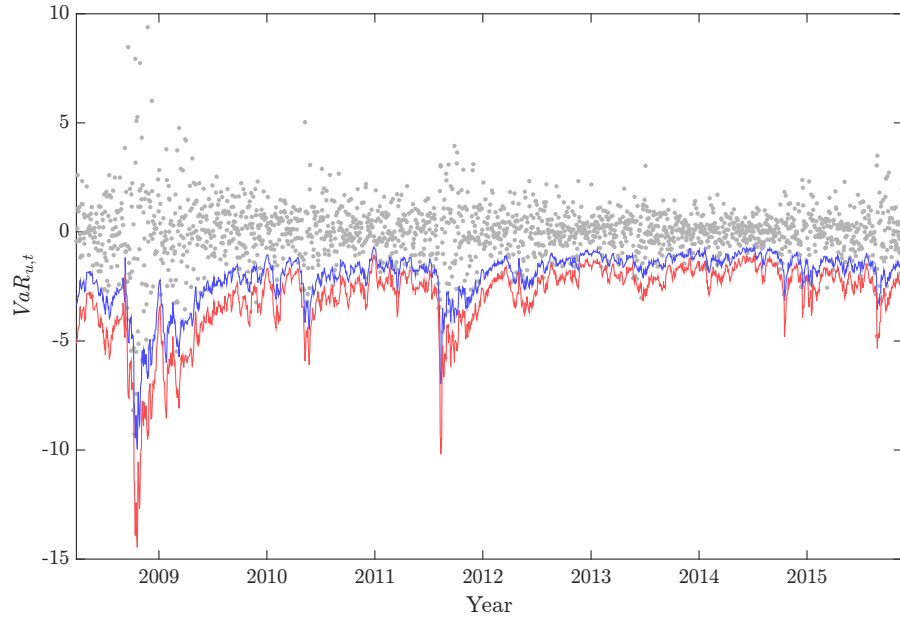


Figure 10: One-step-ahead forecasts of $VaR_{u,t}$ for $u \in \{0.01, 0.05\}$ given by the posterior mean for the FTSE index.

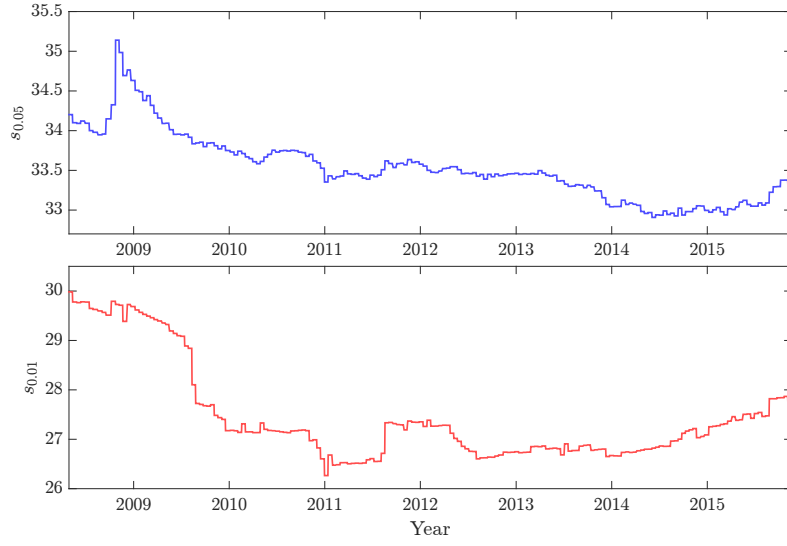


Figure 11: Scaling factors used for the forecasts of $VaR_{u,t}$ for $u \in \{0.01, 0.05\}$ given by the posterior mean for the S&P 500 index.

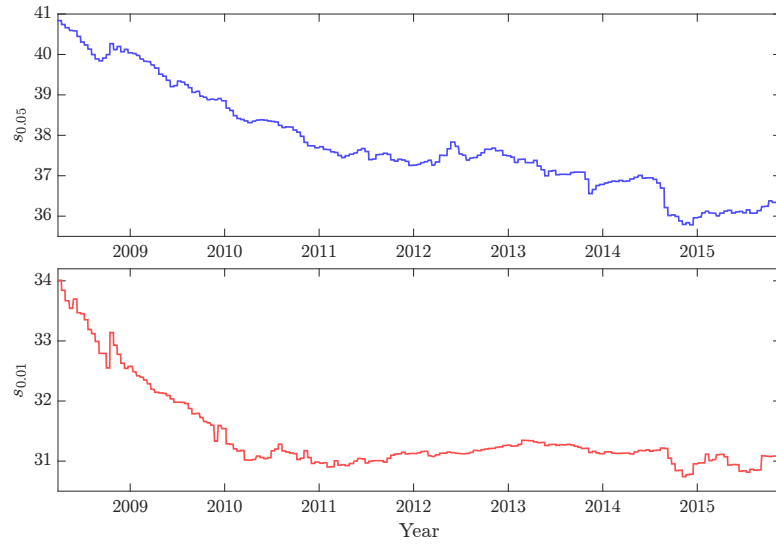


Figure 12: Scaling factors used for the forecasts of $VaR_{u,t}$ for $u \in \{0.01, 0.05\}$ given by the posterior mean for the FTSE index.

	$u = 0.01$		$u = 0.05$	
	SP500	FTSE	SP500	FTSE
CAViaR-SAV	0.0419	0.0367	0.1468	0.1311
GJR-t	0.0384	0.0351	0.1401	0.1301
GJR-skt	0.0375	0.0344	0.1386	0.1294
Realized-t	0.0369	0.0361	0.1355	0.1326
Realized-skt	0.0362	0.0353	0.1340	0.1316
DQF	0.0358	0.0337	0.1339	0.1290

Table 5: Mean values of the scoring function computed from VaR forecasts of the competing models including ours (DQF).

6 Conclusion

Based on the idea of SDA, the main contribution of this paper is to propose the DQF model – a carefully constructed generative model for QF-valued time series. The likelihood function of a QF-valued observation is constructed indirectly by defining a flexible parametric embedding using the g-and-h quantile function. This g-and-h embedding allows us to represent a QF-valued observation as an element in the space of four-dimensional vectors. To perform Bayesian inference, an adaptive MCMC algorithm is designed to sample from the posterior of DQF parameters. The effectiveness of the sampler is demonstrated in a simulation study. Through empirical studies, we show that the DQF model is useful in analysing one-minute returns of major international stock indices. Furthermore, via quantile scaling, the output of the DQF model can be used to provide superior VaR forecasts of daily returns.

7 Acknowledgement

We thank Chris J. Oates for his careful reading of the manuscript and helpful comments. WYC was supported by the Australian Research Council Centre of Excellence for Mathematical and Statistical Frontiers (ACEMS).

References

- Allingham, D., R. King, and K. L. Mengersen (2009). Bayesian Estimation of Quantile Distributions. *Statistics and Computing* 19(2), 189–201.
- Andersen, T. G., T. Bollerslev, F. X. Diebold, and P. Labys (2003). Modeling and Forecasting Realized Volatility. *Econometrica* 71(2), 579–625.
- Arroyo, J., G. González-Rivera, C. Maté, and A. M. San Roque (2011). Smoothing Methods for Histogram-Valued Time Series: An Application to Value-at-Risk. *Statistical Analysis and Data Mining* 4(2), 216–228.
- Bauwens, L. and M. Lubrano (1998). Bayesian Inference on GARCH Models Using the Gibbs Sampler. *The Econometrics Journal* 1(1), 23–46.

- Bosq, D. (2015). Models Associated with Extended Exponential Smoothing. *Communications in Statistics-Theory and Methods* 44(3), 468–475.
- Brownlees, C. T. and G. M. Gallo (2006). Financial Econometric Analysis at Ultra-High Frequency: Data Handling Concerns. *Computational Statistics & Data Analysis* 51(4), 2232–2245.
- Cuevas, A. (2014). A Partial Overview of the Theory of Statistics with Functional Data. *Journal of Statistical Planning and Inference* 147(0), 1–23.
- Delaigle, A. and P. Hall (2010). Defining Probability Density for a Distribution of Random Functions. *The Annals of Statistics*, 1171–1193.
- Demarta, S. and A. J. McNeil (2005). The t Copula and Related Copulas. *International Statistical Review* 73(1), 111–129.
- Engle, R. F. (1982). Autoregressive Conditional Heteroscedasticity with Estimates of the Variance of United Kingdom Inflation. *Econometrica* 50(4), 987–1007.
- Gelman, A., G. Roberts, and W. Gilks (1996). Efficient Metropolis Jumping Rules. *Bayesian statistics* 5(599-608), 42.
- Gerlach, R. and C. W. Chen (2014). Bayesian Expected Shortfall Forecasting Incorporating the Intraday Range. *Journal of Financial Econometrics*, nbu022.
- Gerlach, R. H., C. W. Chen, and N. Y. Chan (2011). Bayesian Time-Varying Quantile Forecasting for Value-at-Risk in Financial Markets. *Journal of Business & Economic Statistics* 29(4), 481–492.
- Gneiting, T. (2011). Making and Evaluating Point Forecasts. *Journal of the American Statistical Association* 106(494), 746–762.
- González-Rivera, G. and J. Arroyo (2012). Time Series Modeling of Histogram-Valued Data: The Daily Histogram Time Series of S&P500 Intradaily Returns. *International Journal of Forecasting* 28(1), 20–33.
- González-Rivera, G. and W. Lin (2013). Constrained Regression for Interval-Valued Data. *Journal of Business & Economic Statistics* 31(4), 473–490.
- Greenwood, J. A., J. M. Landwehr, N. C. Matalas, and J. R. Wallis (1979). Probability Weighted Moments: Definition and Relation to Parameters of Several Distributions Expressible in Inverse Form. *Water Resources Research* 15(5), 1049–1054.
- Hansen, B. E. (1994, Aug). Autoregressive Conditional Density Estimation. *International Economic Review* 35(3), 705–730.
- Harvey, A. and T. Trimbur (2003). Trend Estimation, Signal-Noise Ratios and the Frequency of Observations. In *Proceedings of the 4th Colloquium on Modern Tools for Business Cycle Analysis, EUROSTAT*.

- Harvey, A. C. (1993). *Time Series Models*. MIT Press.
- Haynes, M. and K. Mengersen (2005). Bayesian Estimation of g-and-k Distributions using MCMC. *Computational Statistics* 20(1), 7–30.
- Headrick, T. C., R. K. Kowalchuk, and Y. Sheng (2008). Parametric Probability Densities and Distribution Functions for Tukey g-and-h Transformations and Their Use for Fitting Data. *Applied Mathematical Sciences* 2(9), 449–462.
- Hoaglin, D. C. (1985). *Summarizing Shape Numerically: The g-and-h Distributions*. Wiley Online Library.
- Hosking, J. R. (1990). L-moments: Analysis and Estimation of Distributions using Linear Combinations of Order Statistics. *Journal of the Royal Statistical Society. Series B (Methodological)* 52(1), 105–124.
- Hossain, M. A. and S. S. Hossain (2009). Numerical Maximum Likelihood Estimation for the g-and-k Distribution Using Ranked Set Sample. *Journal of Statistics* 16(1).
- Jondeau, E. and M. Rockinger (2003). Conditional Volatility, Skewness, and Kurtosis: Existence, Persistence, and Comovements. *Journal of Economic Dynamics and Control* 27(10), 1699–1737.
- Koenker, R. and G. Bassett (1978). Regression Quantiles. *Econometrica* 46(1), 33–50.
- Le-Rademacher, J. and L. Billard (2011). Likelihood Functions and Some Maximum Likelihood Estimators for Symbolic Data. *Journal of Statistical Planning and Inference* 141(4), 1593–1602.
- Martens, M. and D. van Dijk (2007). Measuring Volatility with the Realized Range. *Journal of Econometrics* 138(1), 181–207.
- Martinez, J. and B. Iglewicz (1984). Some Properties of the Tukey g and h Family of Distributions. *Communications in Statistics-Theory and Methods* 13(3), 353–369.
- McNeil, A. J., R. Frey, and P. Embrechts (2015). *Quantitative Risk Management: Concepts, Techniques and Tools: Concepts, Techniques and Tools*. Princeton university press.
- Perreault, L., B. Bobée, and P. Rasmussen (1999a). Halphen Distribution System. I: Mathematical and Statistical Properties. *Journal of Hydrologic Engineering* 4(3), 189–199.
- Perreault, L., B. Bobée, and P. Rasmussen (1999b). Halphen Distribution System. II: Parameter and Quantile Estimation. *Journal of Hydrologic Engineering* 4(3), 200–208.
- Peters, G. and S. Sisson (2006). Bayesian Inference, Monte Carlo Sampling and Operational Risk. *Journal of Operational Risk* 1(3), 27–50.

- Peters, G. W., W. Y. Chen, and R. H. Gerlach (2016). Estimating Quantile Families of Loss Distributions for Non-Life Insurance Modelling via L-Moments. *Risks* 4(2), 14.
- Rayner, G. and H. MacGillivray (2002). Numerical Maximum Likelihood Estimation for the g-and-k and Generalized g-and-h Distributions. *Statistics and Computing* 12(1), 57–75.
- Roberts, G. O. and J. S. Rosenthal (2001). Optimal Scaling for Various Metropolis-Hastings Algorithms. *Statistical Science* 16(4), 351–367.
- Taylor, S. J. (2011). *Asset Price Dynamics, Volatility, and Prediction*. Princeton university press.
- Tepper, M. and G. Sapiro (2012). L1 Splines for Robust, Simple, and Fast Smoothing of Grid Data.
- Tepper, M. and G. Sapiro (2013). Fast L1 Smoothing Splines with an Application to Kinect Depth Data. In *Image Processing (ICIP), 2013 20th IEEE International Conference on*, pp. 504–508. IEEE.
- Tsay, R. S. (2010). *Analysis of Financial Time Series*. John Wiley & Sons.
- Tukey, J. W. (1977). Modern Techniques in Data Analysis. In *Proceedings of the NSF-Sponsored Regional Research Conference*.
- Xu, Y., B. Iglewicz, and I. Chervoneva (2014). Robust Estimation of the Parameters of g-and-h Distributions, with Applications to Outlier Detection. *Computational Statistics & Data Analysis* 75(0), 66 – 80.
- Yu, K. and R. A. Moyeed (2001). Bayesian Quantile Regression. *Statistics & Probability Letters* 54(4), 437–447.

A Parameter Blocking Scheme for Sampling

The entire parameter vector $\boldsymbol{\theta} = (\boldsymbol{\theta}_{[1]}, \dots, \boldsymbol{\theta}_{[10]})$ is partitioned into ten blocks as follows:

$$\begin{aligned}
\boldsymbol{\theta}_{[1]} &= (\delta_1, \psi_1, \phi_1), \\
\boldsymbol{\theta}_{[2]} &= (\omega_1, \alpha_1, \beta_1, \eta_1, \lambda_1), \\
\boldsymbol{\theta}_{[3]} &= (\delta_2, \psi_2, \phi_2), \\
\boldsymbol{\theta}_{[4]} &= (\omega_2, \alpha_2, \beta_2, \eta_2, \lambda_2), \\
\boldsymbol{\theta}_{[5]} &= (\delta_3, \psi_3, \phi_3), \\
\boldsymbol{\theta}_{[6]} &= (\omega_3, \alpha_3, \beta_3, \eta_3, \lambda_3), \\
\boldsymbol{\theta}_{[7]} &= (\delta_4, \psi_4, \phi_4, \gamma^*, c), \\
\boldsymbol{\theta}_{[8]} &= (\sigma, \eta_4, \lambda_4, \iota), \\
\boldsymbol{\theta}_{[9]} &= (\mathbf{R}_{2,1}, \mathbf{R}_{3,1}, \mathbf{R}_{4,1}, \mathbf{R}_{3,2}, \mathbf{R}_{4,2}, \mathbf{R}_{4,3}), \\
\boldsymbol{\theta}_{[10]} &= \nu.
\end{aligned}$$

B Additional Material on Signal Ratio

As mentioned in Section 5.3 of the main text, we propose a criteria for measuring the amount of predictable information present in the data conditional on a model. The criteria is similar in spirit to the signal-to-noise ratio (Harvey, 1993; Harvey and Trimbur, 2003) and is termed the signal ratio. Let $\{\xi_t : t \in \mathbb{Z}\}$ be a real-valued covariance stationary process. The signal ratio, denoted by R_{Sig} , is then defined as

$$R_{\text{Sig}} = \frac{\text{Var}[\mathbb{E}(\xi_t | \mathcal{F}_{t-1})]}{\text{Var}(\xi_t)}, \quad (69)$$

where $\mathcal{F}_{t-1} = \sigma(\{\xi_s : s \leq t-1\})$ is the natural filtration. As the conditional mean of an observed noisy process can be interpreted as the underlying single of the process, the numerator of (69) represents the long-run (unconditional) variance of the signal; the denominator is the unconditional variance of the data. It can be shown in general by the *law of total variance* that $R_{\text{Sig}} \in [0, 1)$ if $\text{Var}(\xi_t) < \infty$. Notice that R_{Sig} can be computed for a large class of covariance stationary time series models.

For the rest of the section, we show that the signal ratio is explicitly available for the family of stationary exponential smoothing models, which correspond to the ARMA(1,1) model. Consider the following exponential smoothing model,

$$\begin{aligned} \xi_t &= \mu_t + \epsilon_t, \\ \mu_t &= \delta + \psi \xi_{t-1} + \phi \mu_{t-1}, \end{aligned} \quad (70)$$

where ϵ_t is a *martingale difference*, with $\mathbb{E}(\epsilon_t) = \mathbb{E}(\epsilon_t | \mathcal{F}_{t-1}) = 0$, $\text{Var}(\epsilon_t | \mathcal{F}_{t-1}) = \sigma_\epsilon^2$, and $\text{Var}(\epsilon_t) < \infty$. Using the fact that μ_t and ϵ_t are uncorrelated, the signal ratio can be written as

$$R_{\text{Sig}} = \frac{\text{Var}(\mu_t)}{\text{Var}(\xi_t)} = \frac{\text{Var}(\xi_t) - \text{Var}(\epsilon_t)}{\text{Var}(\xi_t)}. \quad (71)$$

The unconditional variance of ξ_t can be obtained by first rewriting (70) as an ARMA(1,1) model,

$$\xi_t = \delta + (\psi + \phi)\xi_{t-1} - \phi\epsilon_{t-1} + \epsilon_t. \quad (72)$$

Assuming without loss of generality that $\delta = 0$, and using the assumption that $\{\xi_t\}$ is covariance stationary, we can then take the variance of (72) to obtain the unconditional variance Tsay (2010),

$$\text{Var}(\xi_t) = \frac{1 - 2(\psi + \phi)\phi + \phi^2}{1 - (\psi + \phi)^2} \text{Var}(\epsilon_t). \quad (73)$$

By substituting (73) into (71), the explicit expression of the signal ratio is obtained for the model in (70).

$$R_{\text{Sig}} = \frac{\psi^2}{1 - 2\psi\phi - \phi^2}. \quad (74)$$

Notice that the unconditional variance of ϵ_t is cancelled out in the expression, leaving it as a function of only the parameters ψ and ϕ .

Let $\gamma = \psi + \phi$. Using the ARMA(1,1) representation in (72), it can be shown that the

autocorrelation of $\{\xi_t\}$ at lag k , denoted by ρ_k , follows the recursive relationship $\rho_k = \gamma\rho_{k-1}$, for $k \geq 2$ Taylor (2011). It is clear that γ controls the rate of decay of autocorrelations. Thus, the parameter γ is referred to as the persistence level, or memory, of the time series. If $|\gamma| < 1$, the process $\{\xi_t\}$ is mean stationary. This condition is implied to be true by the covariance stationarity assumption.

By letting $\phi = \gamma - \psi$, we can express the signal ratio in (74) in terms of the persistence level γ ,

$$R_{\text{Sig}} = \frac{\psi^2}{1 - \gamma^2 + \psi^2}. \quad (75)$$

It can be seen that

$$\lim_{\psi \rightarrow \pm\infty} \frac{\psi^2}{1 - \gamma^2 + \psi^2} = 1. \quad (76)$$

That is, conditional on a persistence level γ , with $|\gamma| < 1$, the signal ratio converges to 1 as ψ moves away from 0. From (75), it is also apparent that γ controls the rate at which the signal ratio converges to 1. Specifically, when viewed as a function of ψ , the larger the value of γ , the more quickly the signal ratio converges to 1 as $|\psi| \rightarrow \infty$. Figure 13 shows a plot of the signal ratio in (75) as a function of ψ for various levels of persistence.

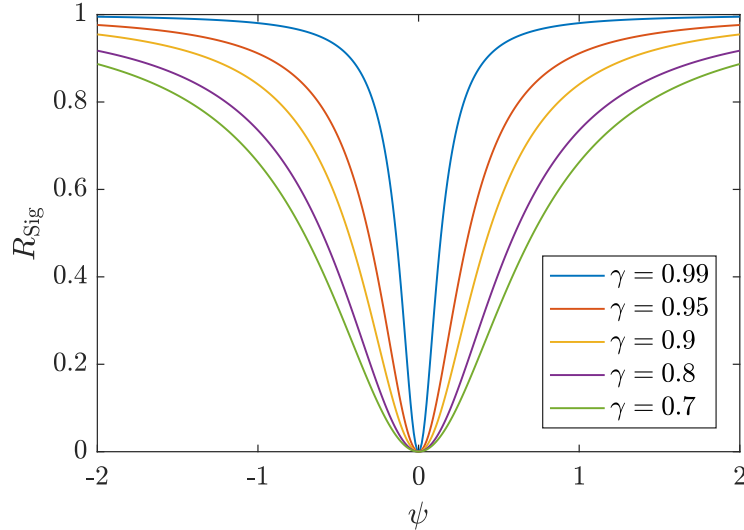


Figure 13: Plot of R_{Sig} as a function of ψ for $\psi \in [-2, 2]$ and $\gamma \in \{0.99, 0.95, 0.9, 0.8, 0.7\}$.

The process $\{\xi_t\}$ is said to be *invertible* if it admits the $\text{AR}(\infty)$ representation,

$$\xi_t = \frac{\delta}{1 - \phi} + \psi \sum_{i=0}^{\infty} \phi^i \xi_{t-1-i} + \epsilon_t. \quad (77)$$

By expanding the recursive definition in (70), it can be shown that $\{\xi_t\}$ is invertible if $|\phi| < 1$. By letting $\psi = \gamma - \phi$ in (75), and considering the cases $\phi = -1$ and $\phi = 1$, the *upper bound* on R_{Sig} for which $\{\xi_t\}$ is invertible can be expressed as a piece-wise linear function of γ . Specifically, if γ is fixed and $|\phi| < 1$, then

$$\sup\{R_{\text{Sig}}\} = \frac{|\gamma| + 1}{2}. \quad (78)$$

C Session Times

	From	To	Start	End
SPX	1996-01-03	2016-05-24	09:30	16:00
DJIA	1996-01-03	2016-05-24	09:30	16:00
Nasdaq	1996-01-03	2016-05-24	09:30	16:00
FTSE	1996-01-03	1998-07-19	08:30	16:30
	1998-07-20	1999-09-17	09:00	16:30
	1999-09-18	2016-05-24	08:00	16:30
DAX	1996-01-03	1999-09-17	08:30	17:00
	1999-09-18	2016-05-24	09:00	17:30
CAC	1996-01-03	1999-09-19	10:00	17:00
	1999-09-20	2000-04-02	09:00	17:00
	2000-04-03	2016-05-24	09:00	17:30
Nikkei	1996-01-03	2006-01-18	09:00	11:00
			12:30	15:00
	2006-01-19	2006-04-23	09:00	11:00
			13:00	15:00
	2006-04-24	2011-11-20	09:00	11:00
			12:30	15:00
	2011-11-21	2016-05-24	09:00	11:30
			12:30	15:00
HSI	1996-01-03	2011-03-06	10:00	12:30
			14:30	16:00
	2011-03-07	2012-03-04	09:30	12:00
			13:30	16:00
	2012-03-05	2016-05-24	09:30	12:00
			13:00	16:00
SSEC	1996-01-03	2016-05-24	09:30	11:30
			13:00	15:00
AORD	1996-01-03	2016-05-24	10:00	16:00

Table 6: History of session times for each of the ten indices. The sample period is from January 3, 1996 to May 24, 2016. For exchanges that have lunch breaks, morning and afternoon session times are recorded on separate lines.

D Robust Outlier Score using Fast L1 Splines

Let $\zeta_t = (\zeta_{t,1}, \dots, \zeta_{t,n_t})$ denote the n_t -dimensional vector of one-minute prices for day t . The corresponding vector of outlier scores $\delta_t \in \mathbb{R}^{n_t}$ is computed by the following steps:

- 1: $\hat{\zeta}_t \leftarrow \arg \min_{\mathbf{z} \in \mathbb{R}^{n_t}} \|\mathbf{z} - \zeta_t\|_1 + \Lambda_1 \|\mathbf{D}\mathbf{z}\|_2^2$
- 2: $\sigma_t \leftarrow \log |\zeta_t - \hat{\zeta}_t|$
- 3: $\hat{\sigma}_t \leftarrow \arg \min_{\mathbf{z} \in \mathbb{R}^{n_t}} \|\mathbf{z} - \sigma_t\|_1 + \Lambda_2 \|\mathbf{D}\mathbf{z}\|_2^2$
- 4: $\varepsilon_t \leftarrow (\zeta_t - \hat{\zeta}_t) \oslash \hat{\sigma}_t$
- 5: $\delta_t \leftarrow |(\varepsilon_t - \text{Median}(\varepsilon_t)) \oslash \text{IQR}(\varepsilon_t)|$

In the above steps, $\|\cdot\|_p$ denotes the L_p norm of a vector, \oslash denotes the Hadamard (element-wise) division, $\text{Median}(\cdot)$ is the sample median operator, and $\text{IQR}(\cdot)$ is the sample interquartile range operator. In steps 1 and 3, we use the fast L1 smoothing splines developed in [Tepper and Sapiro \(2012\)](#) and [Tepper and Sapiro \(2013\)](#) to compute robust nonparametric

approximations to the the intra-daily trend and scale functions. The key feature of the L1 spline is its robustness against outliers. The \mathbf{D} matrix is the standard discrete second-order differential operator, defined as

$$\mathbf{D} = \begin{bmatrix} -1 & 1 & & & \\ 1 & -2 & 1 & & \\ & \ddots & \ddots & \ddots & \\ & & 1 & -2 & 1 \\ & & & 1 & -2 \end{bmatrix}.$$

As pointed out by the authors, the L1 optimisation problems in steps 1 and 3 can be solved very efficiently using the split-Bregman method. The values of the smoothing parameters are $\Lambda_1 = 50$ and $\Lambda_2 = 50000$. Using experiments, we find these values to work well for one-minute equity prices. The important rule-of-thumb here is that the scale function needs to vary much more smoothly than the trend function, i.e., $\Lambda_2 \gg \Lambda_1$, in order to avoid “over-cleaning”.